Clim Dyn (2012) 39:1303–1328
DOI 10.1007/s00382-012-1500-3

Impact of ocean model resolution on CCSM climate simulations

Ben P. Kirtman · Cecilia Bitz · Frank Bryan · William Collins · John Dennis · Nathan Hearn · James L. Kinter III · Richard Loft · Clement Rousset · Leo Siqueira · Cristiana Stan · Robert Tomas · Mariana Vertenstein

Received: 11 May 2011 / Accepted: 16 August 2012 / Published online: 1 September 2012

Abstract The current literature provides compelling evidence suggesting that an eddy-resolving (as opposed to eddy-permitting or eddy-parameterized) ocean component model will significantly impact the simulation of the large-scale climate, although this has not been fully tested to date in multi-decadal global coupled climate simulations. The purpose of this paper is to examine how resolved ocean fronts and eddies impact the simulation of large-scale climate. The model used for this study is the NCAR Community Climate System Model version 3.5 (CCSM3.5)—the forerunner to CCSM4. Two experiments are reported here. The control experiment is a 155-year present-day climate simulation using a 0.5° atmosphere component (zonal resolution 0.625 meridional resolution 0.5°; land surface component at the same resolution) coupled to ocean and sea-ice components with zonal resolution of 1.2° and meridional resolution varying from 0.27° at the equator to 0.54° in the mid-latitudes. The second simulation uses the same atmospheric and land-surface models coupled to eddy-resolving 0.1° ocean and sea-ice component models. The simulations are compared in terms of how the representation of smaller scale features in the time mean ocean circulation and ocean eddies impact the mean and variable climate. In terms of the global mean surface temperature, the enhanced ocean resolution leads to a ubiquitous surface warming with a global mean surface temperature increase of about 0.2 °C relative to the control. The warming is largest in the Arctic and regions of strong ocean fronts and ocean eddy activity (i.e., Southern Ocean, western boundary currents). The Arctic warming is associated with significant losses of sea-ice in the high-resolution simulation. The sea surface temperature gradients in the North Atlantic, in particular, are better resolved in the high-resolution model leading to significantly sharper temperature gradients and associated large-scale shifts in the rainfall. In the extra-tropics, the interannual temperature variability is increased with the resolved eddies, and a notable increases in the amplitude of the El Niño and the Southern Oscillation is also detected. Changes in global temperature anomaly teleconnections and local air-sea feedbacks are also documented and show large changes in ocean–atmosphere coupling. In particular, local air-sea feedbacks are significantly modified by the increased ocean resolution. In the high-resolution simulation in the extra-tropics there is compelling evidence of stronger forcing of the atmosphere by SST variability arising from ocean dynamics. This coupling is very weak or absent in the low-resolution model.

Keywords Climate modeling · Climate variability · Ocean Eddies

B. P. Kirtman (✉) · C. Rousset · L. Siqueira
Rosenstiel School for Marine and Atmospheric Science, University of Miami, Coral Gables, FL, USA
e-mail: bkirtman@rsmas.miami.edu

C. Bitz
Department of Atmospheric Science, University of Washington, Seattle, WA, USA

F. Bryan · J. Dennis · N. Hearn · R. Loft · R. Tomas · M. Vertenstein
National Center for Atmospheric Research, Boulder, CO, USA

W. Collins
University of California, Berkeley, Berkeley, CA, USA

J. L. Kinter III · C. Stan
Center for Ocean-Land–Atmosphere Studies, Calverton, MD, USA

J. L. Kinter III · C. Stan
George Mason University, Fairfax, VA, USA

1 Introduction

There is a growing demand for environmental predictions that include a broader range of space and time scales and that include a more complete representation of physical processes. Meeting this demand necessitates a unified approach that will challenge the traditional boundaries between weather and climate science, and will require a more integrated approach to the underlying geophysical system science and the supporting computational science. One of the consequences of this unified or seamless approach is the need to explore much higher spatial resolution in weather and climate models. This is done to better resolve features, and, more importantly, because capturing the interactions between the various physical and dynamical processes demands this increase in resolution (Randall et al. 2003; Hurrell et al. 2009; Shukla et al. 2009; Brunet et al. 2010). It is also recognized that interactions across time and space scales are fundamental to the climate system itself. The large-scale climate, for instance, determines the environment for microscale (order 1 km) and mesoscale (order 10 km) variability which then feeds back onto the large-scale climate. In the simplest terms, the hypothesis is that the statistics of microscale and mesoscale variability significantly impact the simulation of climate. In typical climate models at, say, 200 km horizontal resolution,[1] these variations occur on unresolved scales, and the micro- and mesoscale processes are parameterized in terms of the resolved variables.

Several recent studies have focused on the importance of *atmospheric* model resolution in the simulation of climate (May and Roeckner 2001; Brankovic and Gregory 2001; Pope and Stratton 2002; Kobayashi and Sugi 2004; Nakamura et al. 2005; Hack et al. 2006; Navarra et al. 2008; Gent et al. 2010). The reported results range from little or no change in the mean and variable climate (i.e., Hack et al. 2006) to significant differences in the cycle of El Niño and the Southern Oscillation (ENSO; Navarra et al. 2008) and in sea surface temperature (SST) biases in the upwelling regions (i.e., Gent et al. 2010).

The Gent et al. (2010; hereafter G10) study is of particular relevance here, and there is much discussion throughout this paper comparing the results from our simulations with the findings of G10. First, both studies used the same version of the National Center for Atmospheric Research (NCAR) Community Climate System Model (CCSM). Second, the "high-resolution" model (referred to as 0.5° CCSM3.5) used by G10 is identical to the control model used here. Third, while G10 focused on atmospheric model resolution (e.g., 2° vs. 0.5° horizontal resolution), the emphasis here is on ocean model resolution. We enhanced the 1° ocean model resolution used by G10 to 0.1°. The atmospheric component model resolution is identical (i.e., 0.5°) in all the experiments presented here.

McClean et al. (2011) and Bryan et al. (2010) were the first to examine the question of resolution dependence of simulations with CCSM that incorporated an eddy-resolving ocean component.[2] In particular, McClean et al. (2011) used the same version of the CCSM component models as used in this study and G10 but with approximately a 0.25° horizontal atmospheric model resolution coupled to the 0.1° ocean component. The coupled model was run for 20 years, and produced simulated SST that is too cold in the sub-polar and mid-latitude Northern Hemisphere, but more realistic Aghulas eddy pathways compared to ocean-only simulations at comparable resolution. Bryan et al. (2010) examined the McClean et al. (2011) simulation and conducted two additional experiments separately probing the ocean and atmospheric model resolution. As in McClean et al. (2011), the Bryan et al. (2010) simulations were run for approximately 20 years. Bryan et al. (2010) focused primarily on the coupling between the lower atmosphere and the SST, and found a more realistic pattern of positive correlation between high-pass filtered surface wind speed and SST when the ocean component model is eddy resolving. Both of these earlier studies are viewed as predecessors for the present work. The fundamental difference is that the focus of this work is on climate variability, which requires simulations that extend well beyond 20 years.

The motivation for our study is to determine how increased ocean model resolution impacts the simulation of the large-scale climate variability. As such, in this paper, we focus on relatively large-scale features—a more regional focus will be described in subsequent papers—and require simulations that are on the order of 50–100 years. The current literature provides compelling evidence suggesting that an eddy-resolving ocean component model will significantly impact the simulation of the large-scale climate, although multi-decade to century length experiments in this resolution regime are, as yet, very limited in number. For example, Delworth et al. (2012) compare simulations with versions of the GFDL coupled climate model with eddy-resolving, eddy-permitting, and eddy-parameterized resolutions. They find systematic improvements in many aspects of the climate with increasing resolution, though subsurface ocean temperature drift may be exacerbated in the eddy-permitting regime when eddy heat transports are neither properly resolved nor parameterized.

[1] Throughout this paper, model "resolution" refers to the spacing of model grid elements.

[2] In common parlance, *eddy-resolving* models have horizontal resolution of less than 1/6°, in contrast to *eddy-parameterized* models with 1° or greater grid spacing or *eddy-permitting* ocean models whose resolution lies between 1/6° and 1°.

Minobe et al. (2008; hereafter M08) performed two high-resolution AGCM simulations—one using high resolution SST and the other with degraded or smoothed SST. The ability to resolve the sharp SST gradients associated with the Gulf Stream significantly affected the large scale AGCM simulated rainfall. Maloney and Chelton (2006) examined the SST-wind stress coupling (Chelton et al. 2001) in the Coupled Model Intercomparison Project (CMIP3) database and found that the ability to capture the observed coupling degrades with coarsening resolution. Bryan et al. (2010) examined wind speed-SST coupling in their high-resolution simulations and found that, over much of the globe, resolving the ocean fronts and eddies (as opposed to increased atmospheric model resolution) was required to capture the observed relationship. Jochum et al. (2007) and Roberts et al. (2009) showed that tropical instability waves (TIW) have the potential to significantly alter tropical atmospheric variability and teleconnection patterns in precipitation extending into the extratropics, and that climate models underestimate extreme events when TIW are not taken into account. An (2008) argues that TIW are a negative feedback on ENSO that can possibly explain the asymmetry between warm and cold events.

The remainder of this paper is organized as follows. Section 2 describes the model configuration, experimental design and the initialization of the climate simulations. Some details regarding the numerical implementation are provided, as substantial innovation was required. The drift or spin-up is diagnosed in Sect. 3 primarily in terms of area-averaged quantities. The surface temperature appears to reach equilibrium after 100 years, but we also show that significant sub-surface ocean drift remains throughout the simulations. Section 4 presents global maps of the annual mean and the annual cycle along the equator. Here we focus on a 50-year period after the surface climate appears to have reached equilibrium. As such, the emphasis is on near surface climate variables, e.g., surface temperature and precipitation. We also focus on the near surface climate in the Gulf Stream region, as this is an area we expect a large impact associated with the resolved eddies. Section 5 shows results from the sub-surface ocean and changes in the sea-ice extent. An explanation of the origins of the ubiquitous warming in the eddy resolving simulation is provided in Sect. 6. Finally, the impact of the increased ocean resolution in terms of tropical interannual variability and air-sea interactions is discussed in Sect. 7 and concluding remarks are provided in Sect. 8.

2 Model configure and experimental design

2.1 CCSM3.5

The model used for this study is a pre-release NCAR Community Climate System Model version 4.0. While it has the same scientific configuration as CCSM version 3.5 (Neale et al. 2008; G10), it has a significantly upgraded software infrastructure. The new CCSM 4.0 infrastructure enables very-large-scale parallelism to achieve the coupling of ultra-high-resolution component models (Dennis et al. 2012). The atmospheric component model, the Community Atmospheric Model (CAM) is based on a finite volume discretization (Lin and Rood 1997) rather than the spectral discretization of the governing equations used in earlier versions of CAM, and has extensive changes in the parameterization of sub-grid-scale processes that have resulted in a significant improvement in the simulation of tropical variability relative to CCSM3.0 (Neale et al. 2008). Changes in the other component models, while less extensive, have also contributed to a reduction in systematic biases (Jochum et al. 2008; G10).

All the component models communicate via the CCSM flux coupler (Craig et al. 2011; Craig et al. 2005). In all the experiments, the fluxes at the air-sea interface are calculated at 6-h intervals using atmospheric state variables interpolated onto the ocean model grid, and conservatively remapped back onto the other component model native grids. In all the experiments described here, the surface stress is computed from the relative motion of the surface atmospheric winds and ocean currents, which has been shown to reduce coupled model biases (Luo et al. 2005). This provides an additional potential feedback process between ocean mesoscale variability and low level atmospheric flow (e.g., Small et al. 2009), though we do not address this issue here.

2.2 Increasing the ocean model resolution

As noted in the introduction, the objective of the numerical experiments is to examine how resolved ocean fronts and eddies impact the large-scale climate. Two experiments are reported here. The first experiment (i.e., control, referred to as LRC) is a 155-year present-day climate simulation of the 0.5° atmosphere (zonal resolution 0.625°, meridional resolution 0.5°; the land component has the same resolution) coupled to ocean and sea-ice components with zonal resolution of 1.2° and meridional resolution varying from 0.27° at the equator to 0.54° in the mid-latitudes on a dipole grid (Murray 1996). This control experiment is nearly identical to the "high-resolution" experiment in G10 in terms of the model configuration, but differs in its initial state and climate forcing. The G10 experiment was a transient climate simulation initialized with a state extracted from a coarser resolution twentieth century integration at year 1980. The initial condition for our experiments was taken from the end of a previously completed present day control simulation carried out with an earlier version of CCSM, so that the ocean state is fully

"spun-up" and the initialization shock ought to be minimized; however, as will be shown, some climate drift is apparent. The one difference in model configuration from G10 is that the vertical resolution in the ocean component is reduced from 60 to 42 levels in order to match that used in the high-resolution experiment described next. The second simulation is carried out in two phases with the same atmospheric and land surface models coupled to 0.1° ocean and sea-ice component models. The ocean model configuration in this case is identical to that used in a century-long ocean simulation (Maltrud et al. 2010) and in the coupled climate simulation of McClean et al. (2011). The model has grid poles in North America and Asia (Murray 1996). The maximum grid spacing is 11 km at the equator, reducing to 2.5 km at high latitudes. In addition to the change in horizontal resolution from the control experiment, there are commensurate changes in the parameterization of horizontal sub-grid scale dissipation. The high-resolution model uses a biharmonic closure for both momentum and tracers. The hyper-viscosity and diffusivity are scaled with the cube of the local grid spacing as described in Bryan et al. (2007). The initial condition for the first phase (referred to as HRC03). is the same as the control simulation except that the ocean state has been interpolated to the 0.1° grid. This interpolation leads to a significant period of adjustment (see below). The second phase (referred to as HRC06) begins at year-102 of HRC03 using the same resolution and parameters except in this case the polar winds have been filtered to reduce computational instability. This phase of the experiment extends to year-155. We have conducted a detail analysis of this overlap period and have compared years 70–112 of HRC03 to years 102–152 of HRC06. Based on our analysis we conclude that the polar filter produces statistically significant differences at the 99 % confidence interval between to the two high-resolution simulations. However, the differences between the two high-resolution simulations are very small compared to the differences between high-resolution simulations and the low-resolution simulation. The analysis herein (except for documenting the spin-up) focuses on the 50 years of overlap between HRC06 and LRC. The experiments discussed above are summarized in Table 1.

As a point of information, the computational costs for the simulations are as follows. The LRC simulation requires 13 K CPU hours per simulated year and the HRC06 simulation requires 77 K CPU hours per simulated year.

3 Spin-up

Figure 1a shows the global mean SST anomaly (averaged over grid-boxes whose ocean fractional coverage is greater than 50 %) from the beginning of the simulation to the end of year-155. The anomaly is defined as the difference from the monthly mean climatology calculated from the last 50 years of each respective simulation. The LRC simulation (shown in red) includes all 155 years, whereas HRC03 extends from year-1 to year-112 (shown in black), and HRC06 (shown in blue) includes years 102–155. The last 50-year monthly climatology is shown in Fig. 1b. In Fig. 1b we omit HRC03 since the differences between HRC06 and HRC03 are indistinguishable compared to the differences between HRC06 and LRC. Despite the fact that the initial conditions are drawn from the same data there is a significantly different initial evolution in the LRC and HRC03 simulation. Beyond about year 50, both LRC and HRC03 appear to have similar statistics in the global mean SST variability despite rather different mean climates. Figure 1a also indicates that HRC06 and HRC03 have similar climates beyond about year 50. Finally, we see that the annual cycle for HRC06 (or equivalently HRC03) is about 0.2–0.3 °C warmer than LRC (Fig. 1b). This is in contrast to G10 where the increase in *atmospheric* resolution leads to upper-ocean cooling of about the same magnitude. Essentially, much of the global cooling due to increased atmospheric resolution in G10 (see their Fig. 2) is reversed by increasing the ocean resolution. Finally, we note that both simulations are considerably warmer than the observational estimates from the Advanced Very High Resolution Radiometer (AVHRR; clear sky derived SST data monthly gridded from Jan 1985 to Dec 2002 were averaged to produce monthly SST climatology on ~9 km global lat/lon grid; Casey et al. 2010).

While it appears that the globally averaged surface temperature reaches equilibrium (or at least the drift is small) by year 70 or 80, the deep ocean temperatures continue to drift. Here we define the drift in terms of annual mean temperatures as a function of depth. The drift for any year, therefore, is the difference from the year 1 annual

Table 1 Model resolution experiments with CCSM family of models

Study	Atmos (degrees)	Ocean (degrees)	Experiment
Gent et al. (2010)	0.5	1.2 × (0.27–0.54)	Climate of the twentieth century
Bryan et al. (2010)	0.25	0.1 × 0.1	20-year simulation with fixed forcing
McClean et al. (2011)	0.25	0.1 × 0.1	20-year simulation with fixed forcing
Current study	0.5	0.1 × 0.1	155-year simulation with fixed forcing

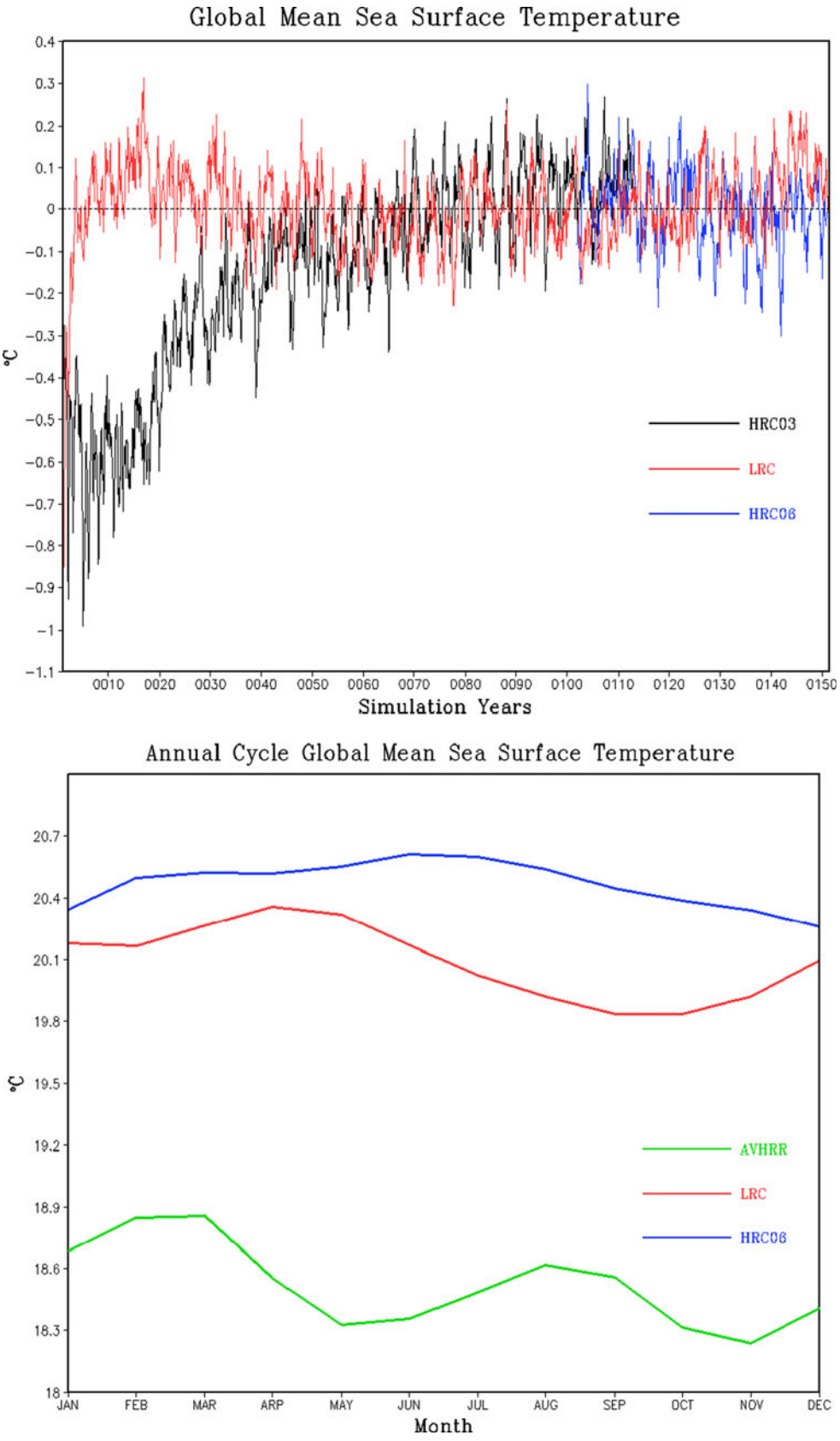

Fig. 1 Time evolution of global mean sea surface temperature anomalies (*top*) for LRC (*red*), HRC03 (*black*) and HRC06 (*blue*). The anomaly is defined as the deviation from the climatology based on the last 50-years of each respective simulation. The *bottom panel* shows the last 50-year monthly mean climatology from LRC (*red*), HRC06 (*blue*) and AVHRR Climatology (*green*)

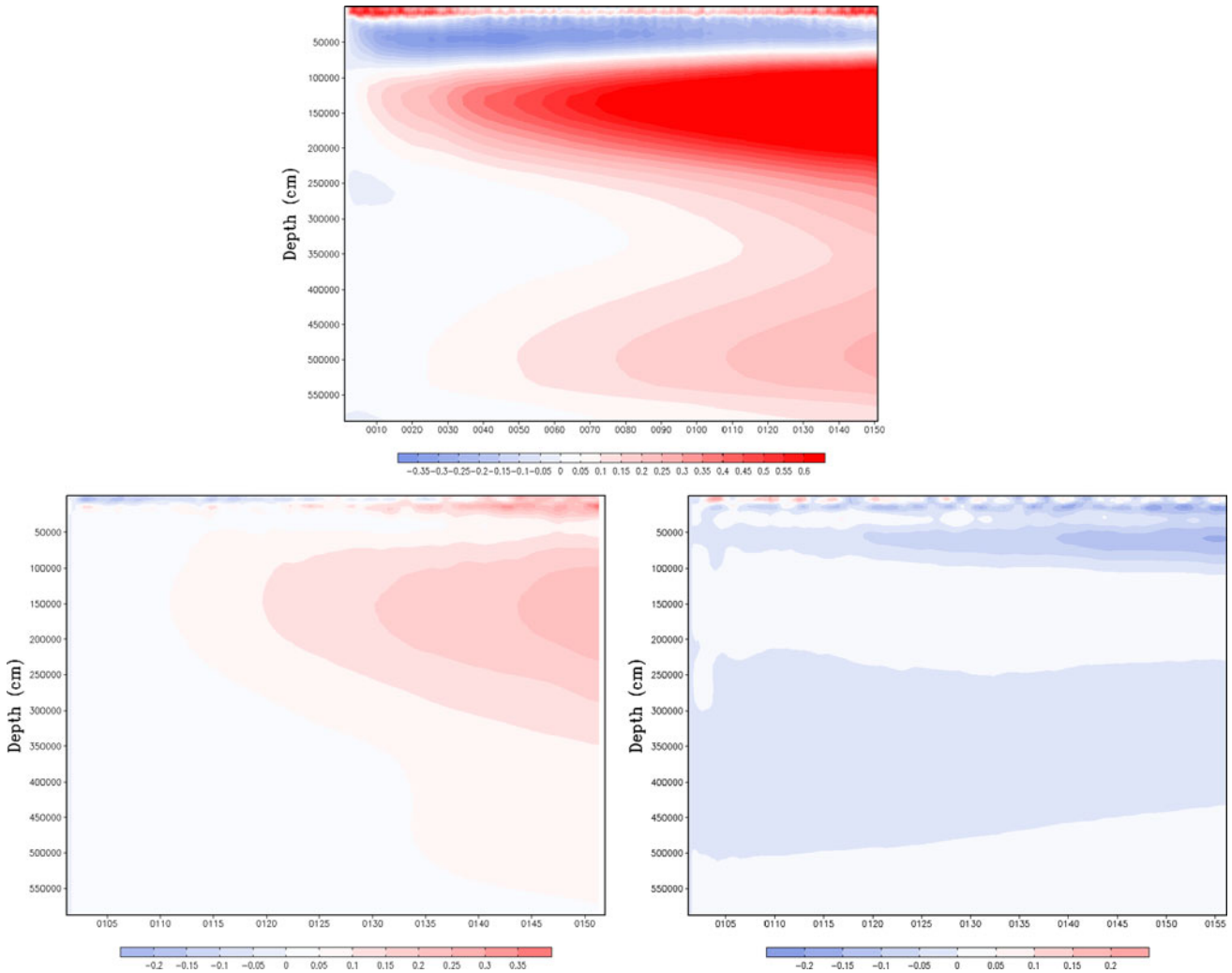

Fig. 2 Global ocean temperature drift as a function of depth and time. *Top panel* shows the drift for LRC in °C where the drift is defined as the difference (current year minus year 1) in the annual mean. For example, Fig. 2 (top) shows the global mean ocean subsurface temperature drift for all 155 years of LRC as a function of depth. In the upper 500 m the ocean temperatures stabilize in the first 40–50 years, while below 500 m the drift continues throughout the simulation. In order to compare the drift in in LRC and HRC06 we have redefined the drift relative to year-102 instead of year 1. The bottom two panels of Fig. 2 show the drift for years 102–155 for LRC (left panel) and HRC06 (right panel). The deep ocean drift in LRC remains apparent and there is some upper ocean (above 500 m) low frequency variability that can also be detected in the top panel of Fig. 2. In contrast to LRC, the drift in HRC06 is weaker and more surface intensified compared to LRC, with cooling at all depths. Note that the pattern of surface cooling and subsurface warming in LRC is very similar to that described in the experiments of Delworth et al. (2012), which they attribute to eddy heat transports that are too weak.

4 Annual mean and annual cycle

4.1 Near surface temperature

Figure 3 (top panel) shows the annual mean SST (displayed on the atmospheric model grid for cells with fractional land and sea ice coverage less than 50 %) difference between HRC06 and LRC01, and the bottom panels of Fig. 3 show the differences from observational estimates that is LRC-OBS and HRC06-OBS respectively. The HRC06 SST is warmer than LRC01 throughout the extratropics. The relative warmth of HRC06 is quite large in the

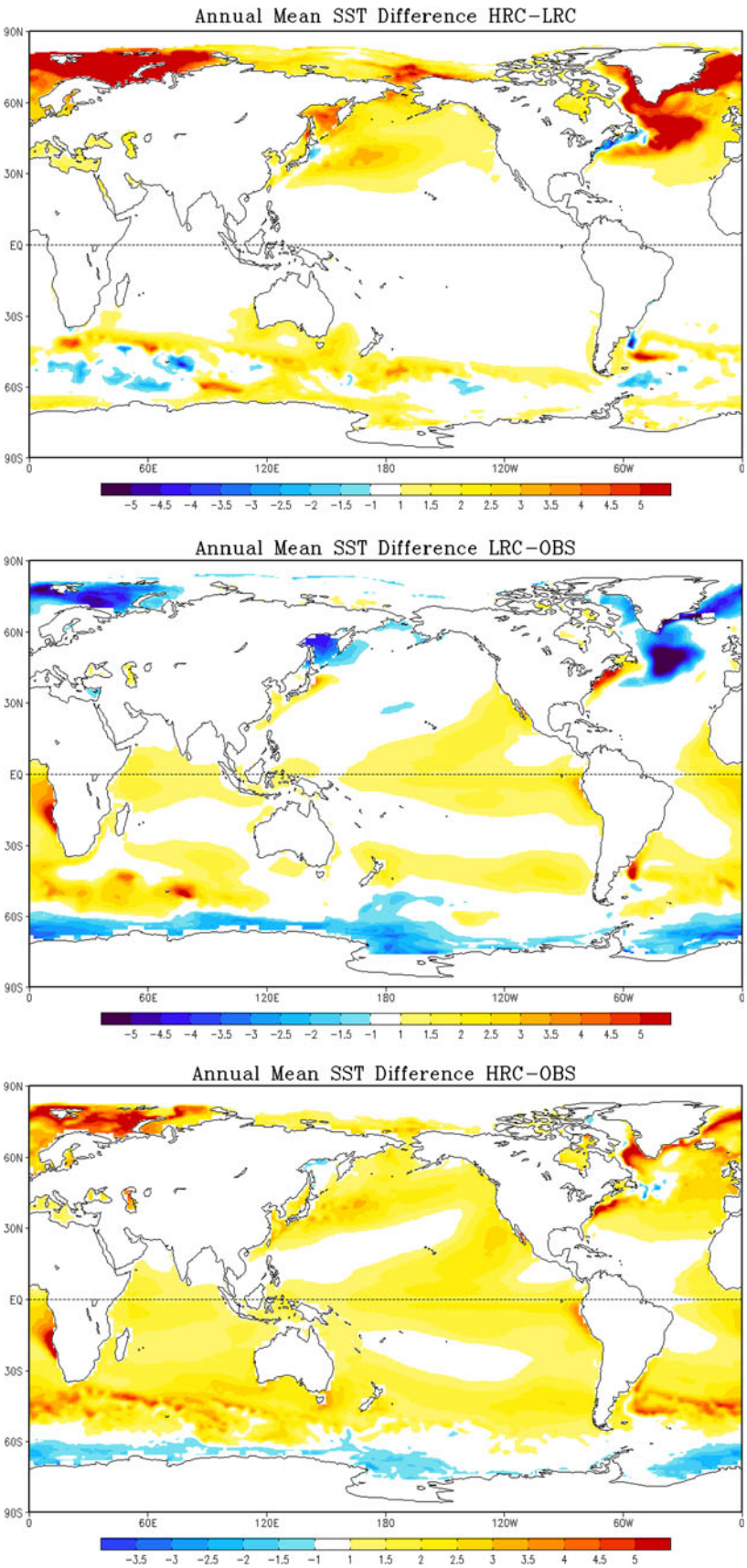

Fig. 3 Annual mean surface temperature difference (*top*) HRC06-LRC, (*middle*) LRC-Observations and (*bottom*) HRC06-Observations. Observational estimates are based on AVHRR climatology. Contour is in degrees Celsius. Values plotted are statistically significant at 99 % confidence interval using a standard Student's *t* test

North Atlantic and the North Pacific, and is also concentrated in the western boundary current regions and the Southern Ocean. A similar, but smaller response to increasing ocean component resolution was obtained in the U.K. HiGEM model (Shaffrey et al. 2009). Much of the warming along the North Atlantic Current is a result of a westward shift of the subpolar front to a more realistic position, resulting in an amelioration of the large negative SST bias typical of coarse resolution models in that region. The dynamics of the North Atlantic current in this region are complex, and the solutions, even at this high-resolution, remain sensitive to parameterization choices (Bryan et al. 2007). As shown in that study, the path of the Gulf Stream and North Atlantic current depend on a complex interaction of the surface and deep boundary currents, and thus can be influenced by factors such as the stability of the Gulf Stream after it separates from the coast (stronger instability leading to a stronger barotropic flow and interaction with topography), and the strength and depth of the southward flowing deep western boundary current. It is difficult to isolate causality in these experiments with the output available. There are large positive differences in the northern North Atlantic in Fig. 3 (top), especially where sea ice concentrations approach 50 %. Although not seen with this contour interval there is ubiquitous warming throughout the tropics, but the magnitude of the warming is generally between 0.25 and 0.75 °C. There are some notable reductions in error in HRC06 relative to LRC. These reductions include the North Atlantic, the Sea of Okhotsk and the Southern Ocean south of 60S.

The annual mean land and sea ice surface temperature (again displayed on the atmospheric model grid, for cells with fractional land and sea ice coverage greater than 50 %) is shown in Fig. 4. One might expect that the land surface response would be relatively small since only the ocean resolution is different. However global average SST has a large impact on global land temperatures as shown in atmosphere-only simulations with prescribed SST (Scaife et al. 2008). The warming in the sea-ice regions is notable. Much of the surface where there should be perennial Arctic sea ice in the HRC06 simulation is over 5.0 °C warmer than LRC. Sea-ice issues are discussed further below. The relative warmth (HRC06-LRC) of the land surface in much of the Northern Hemisphere exceeds 1.0 °C. This is consistent with the results of Deser et al. (2010) who found that heat released from the Arctic Ocean under reduced sea-ice conditions is communicated to the Arctic atmospheric boundary layer by transients, and Kumar et al. (2010) who found that arctic sea-ice loss during 2007 accounted for a large fraction of high-latitude land surface warming north of 60 N. The warming of the Southern Hemisphere land surface is small except in the Antarctic.

Figure 5 (top) shows the atmospheric temperature difference at 850 hPa along with estimated model errors in LRC (middle) and HRC06 (bottom). Observational estimates of 850 mb temperature are from NCEP/NCAR reanalysis (Kalnay et al. 1996). Throughout the entire lower troposphere HRC06 is warmer than LRC. This relative warmth holds even over regions where some surface cooling was noted, e.g., regions in the Southern Ocean

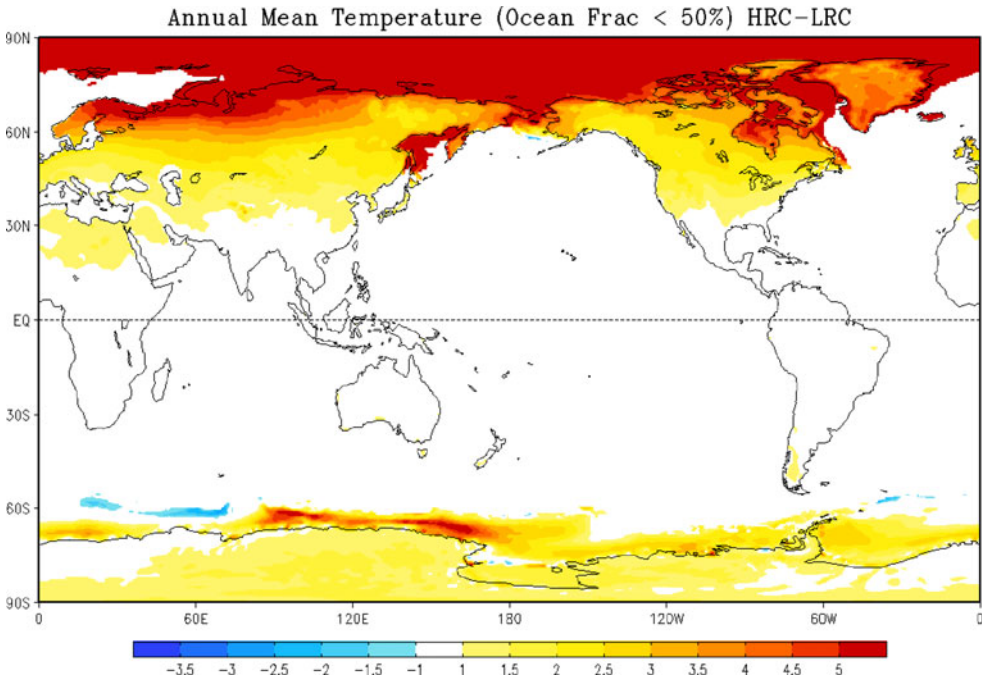

Fig. 4 Annual mean surface temperature (fractional land and sea ice coverage greater than 50 % in a grid cell) difference (HRC06-LRC). Contours are in degrees Celsius. Values plotted are statistically significant at 99 % confidence interval using a standard Student's *t* test

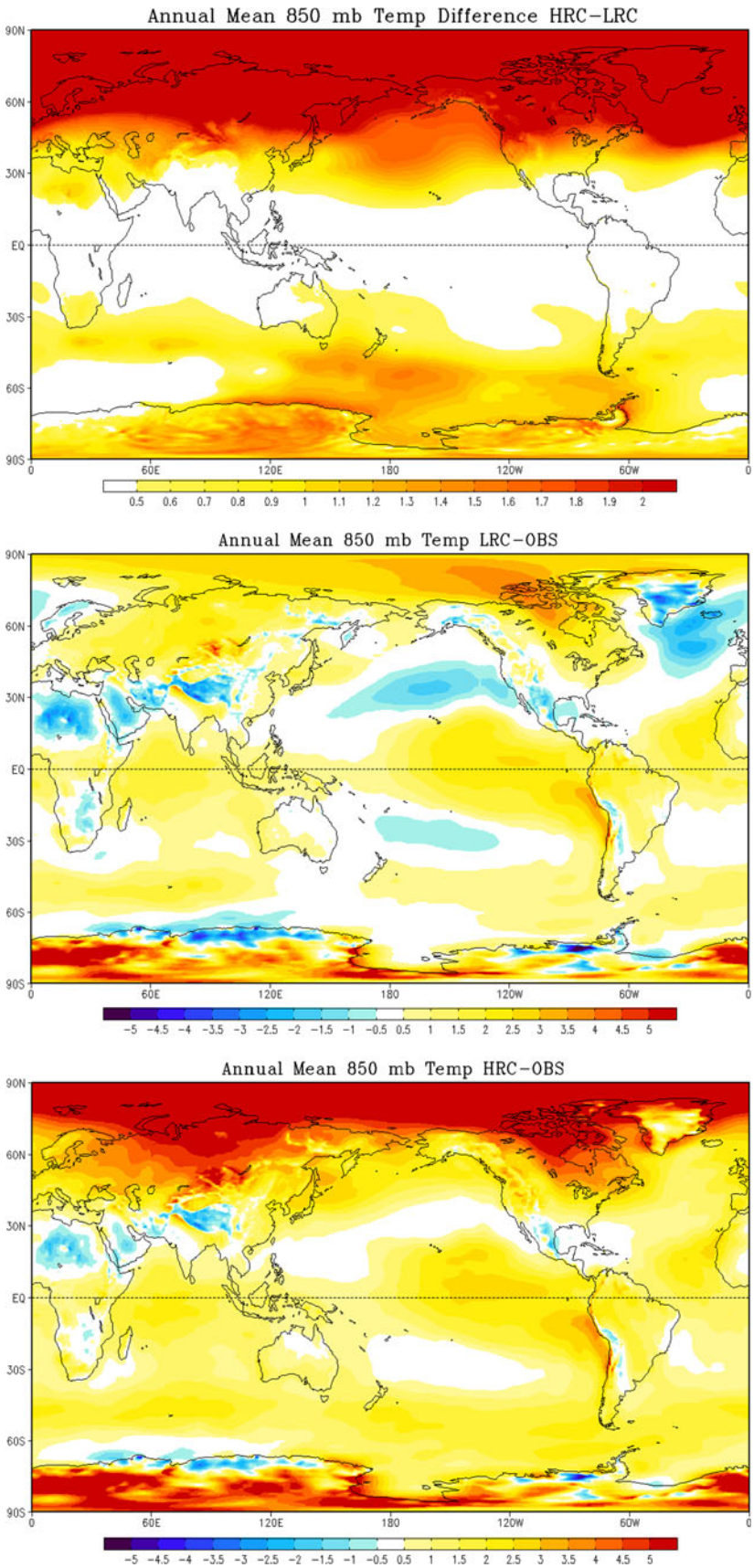

Fig. 5 (*Top*) Annual mean 850 mb temperature difference (HRC06-LRC), (*middle*) LRC-observations and (*bottom*) HRC06-observations. Observational estimates are from NCEP/NCAR reanalysis (Kalnay et al. 1996). Contours are in degrees Celsius. Values plotted are statistically significant at 99 % confidence interval using a standard Student's *t* test

centered on 60°S (see Fig. 3). The regions of relatively large surface warming are associated with corresponding lower tropospheric warming. The 850 hPa temperature errors are largely consistent with the surface temperature errors seen in Fig. 3. Perhaps somewhat different is the amelioration of the sub-tropical Pacific cold biases. Overall, however, the warm errors in the high-latitudes in HRC06 dominate the error maps.

4.2 Precipitation

The annual mean precipitation difference (HRC06-LRC) is shown in Fig. 6 (top). The total fields are shown in Fig. 6 (middle) and observational estimates are shown in Fig. 6 (bottom). The observational estimates are based on Xie and Arkin (1997) analysis commonly referred to at as CMAP. In the extra-tropics, the rainfall increases with increasing ocean model resolution in the regions overlying western boundary currents and the Southern Ocean near South Africa. These differences can also be detected in the total fields (Fig. 6 middle). This is consistent with regions of relatively large western boundary current temperature differences, as shown in Fig. 3. The precipitation in HRC06 increases over LRC in high-latitude ice regions where HRC06 is relatively warm (see Fig. 3). There are also precipitation differences in the tropical Pacific, which are significant at the 99 % confidence interval and yet are difficult to detect in the total fields. The rainfall increases in the central and eastern Pacific slightly north of the equator, and there is reduced rainfall in the western Pacific also slightly north of the equator. The east–west rainfall differences in the tropical Pacific are consistent with a stronger ENSO and a weaker Walker circulation (see Fig. 18 and associated discussion). Finally, there are some regional differences over land that are worth noting. For example, the rainfall over equatorial South America is reduced.

The mechanism for the intensification of the east Pacific ITCZ is not fully understood, but one possible mechanism is related to the sea-ice changes (see also Sect. 6). HRC06 has significantly less sea-ice compared to LRC in the Northern Hemisphere, which as suggested by Chiang and Bitz (2005; see also Kang et al. 2008), should lead to an intensification of the ITCZ in the warmer Hemisphere (i.e., Northern Hemisphere) as detected in Fig. 6 (top) in the eastern Pacific. It is also possible that resolved TIW in HRC06 produce relative SST warming slightly north of the equator, which serves to strengthen the ITCZ. The ITCZ is also seen to intensify in the Northern Hemisphere in the Atlantic Ocean, particularly with noted reduction of rainfall in the Southern Hemisphere—again hypothesized to be consistent with relatively stronger warming on the Northern Hemisphere high latitudes.

4.3 Gulf stream region

One of the key motivating factors for this study is to assess how resolved ocean fronts and eddies impact the mean large-scale climate, through mechanisms described, for example, by M08. We have applied some of the M08 diagnostic methods in Figs. 7, 8, 9. Specifically, Fig. 7 (top) shows the North Atlantic SST climatology from HRC06 (shaded) and LRC superimposed (black contours) and Fig. 7 (bottom) shows the observational estimates from AVHRR. Figure 8 is in the same format, except the figure shows the climatological rainfall, and Fig. 9 shows the surface current speed calculated from monthly means. The observational estimate of surface current speeds are from Maximenko and Hafner (2010)[3] and CMAP is used to estimate the observed rainfall climatology. In terms of the surface temperature, HRC06 produces much sharper gradients than LRC along the coast of North America and in the Gulf Stream separation region (see Fig. 7). Comparisons with the observational estimates highlight the fact that the HRC06 simulation is far more realistic even in the detailed structure to the south and east of Newfoundland. In contrast, the SST in the LRC simulation is strikingly similar to the smoothed (and degraded SST) used in the prescribed SST AGCM simulations in M08. Note that fields plotted in both Figs. 7, 8 are on the AGCM grid, which is the same in HRC06 and LRC.

Figure 8 indicates significant structural changes in the simulated rainfall associated with ocean model resolution. For example, the axis of maximum rainfall in HRC06 follows the maximum SST gradient so that the rainfall hugs the US coast and extends out into the open Atlantic as part of the Gulf Stream extension. The LRC simulation captures some aspects of the rainfall maximum along the US coast, but perhaps as expected, fails to capture the east–west oriented maximum along the Gulf Stream extension. Rainfall in the HRC06 simulation bears a striking resemblance to the observational estimates.

Figure 9 shows the surface current speed in HRC06 (shaded) and in LRC (contours). The surface current speed is calculated from monthly mean data using the same overlapping 50-year period. The improvements in the structure and amplitude of the surface current speed are striking. The Gulf Stream separation in HRC06 is easily detected and extends well into the open ocean, whereas in LRC the coastal currents are weak and less than 20 cm s^{-1} in broad regions where the HRC06 currents are twice as strong. Many of the complexities of the currents in the Labrador Sea and immediately to the south in the HRC06 simulation are absent in LRC.

[3] See http://apdrc.soest.hawaii.edu/datadoc/scud.php.

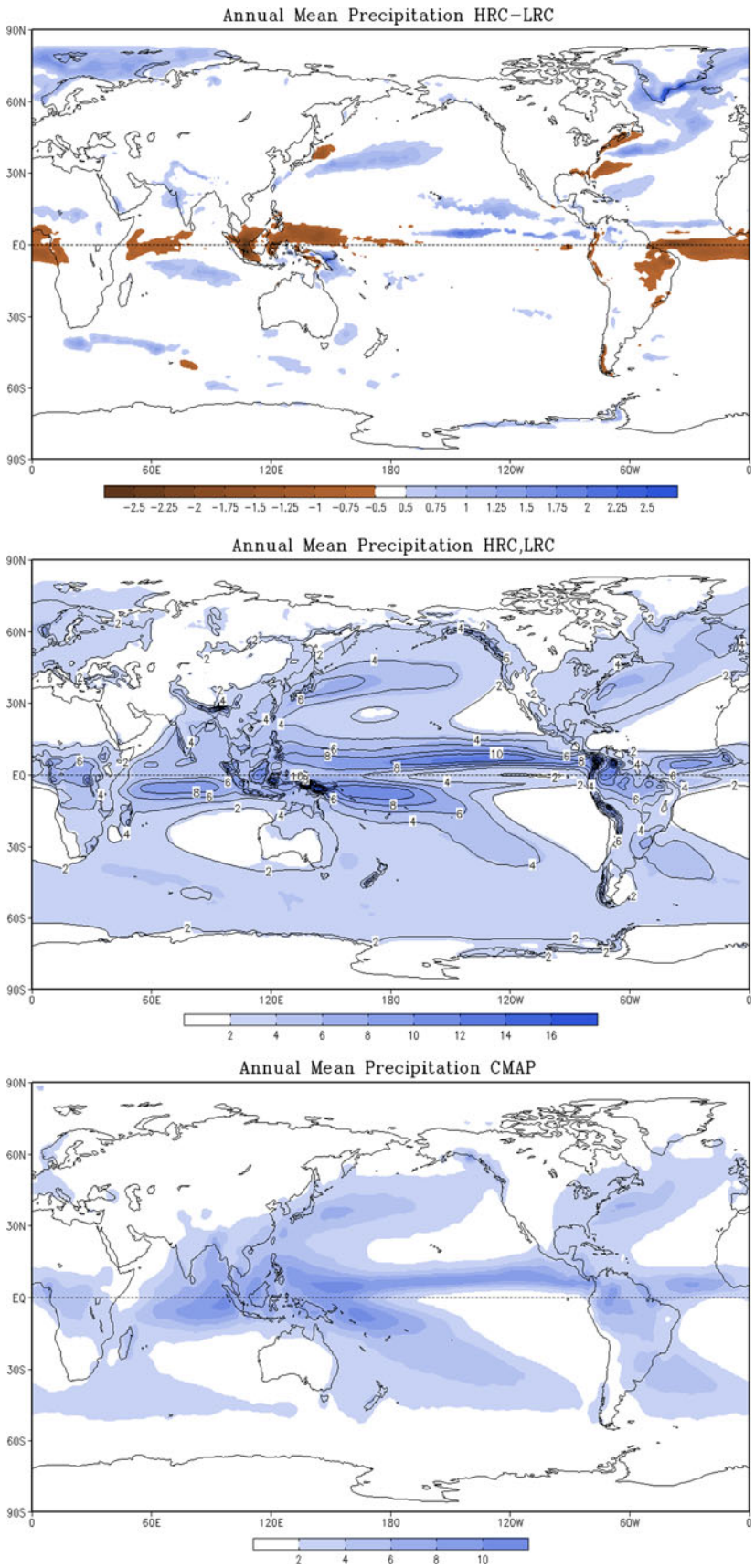

Fig. 6 (*Top*) Annual mean precipitation difference (HRC06-LRC), (*middle*) annual mean precipitation for HRC06 (*shaded*) and LRC (*contours*), and (*bottom*) observational estimates from Xie and Arkin (1997). Values plotted are statistically significant at 99 % confidence interval using a standard Student's *t* test. *Shading* and *contours* are in mm day^{-1}

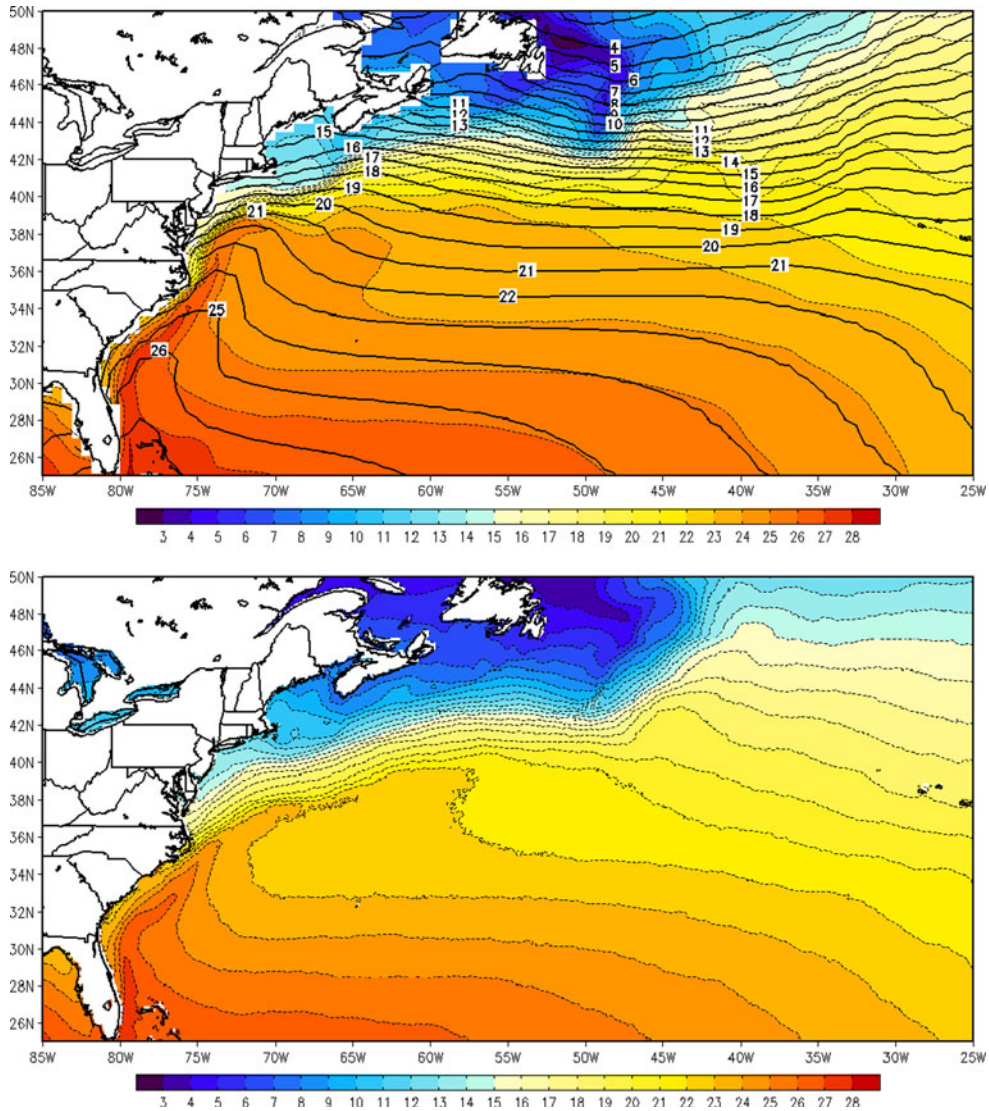

Fig. 7 The top panel shows the time mean SST temperature in °C from LRC (*contours*) and HRC06 (*shaded*). The *bottom panel* shows climatological SST from AVHRR

Similar results and improvements with HRC06 as those shown in Figs. 7, 8, 9 are also found in the Kuroshio region of the North Pacific.

4.4 Equatorial annual cycle

In much the same way that resolving ocean mesoscale fronts and eddies motivated the numerical experiments presented here, resolving TIW was also expected to modify the near equatorial climate. Jochum and Murtugudde (2004), for example, argue that the presence of TIW leads to a net heat gain slightly poleward of the equator. Relative warming slightly north of the equator has been detected in HRC06 in both the Pacific and to a lesser degree in the Atlantic (Fig. 3). TIW have typical wavelengths of 10° in longitude so that we expect the control simulation (LRC) to capture significant TIW variability, but as we indicate here there are notable difference. The differences in the TIW activity between LRC and HRC06 show two distinct elements. First, the warming signal in HRC06 relative to LRC reduces the strength of the eastern Pacific cold tongue and the associated meridional SST gradient. This results in fewer periods where TIW activity is relatively large in HRC06 compared to LRC. Second, the active TIW periods in HRC06 when compared to active TIW periods in LRC have larger amplitude. These differences are highlighted in Fig. 10, which shows time-longitude sections of Pacific daily SST averaged from 3°N to 6°N for both HRC06 (left panel) and LRC (right panel). These 10-year periods were chosen at random.

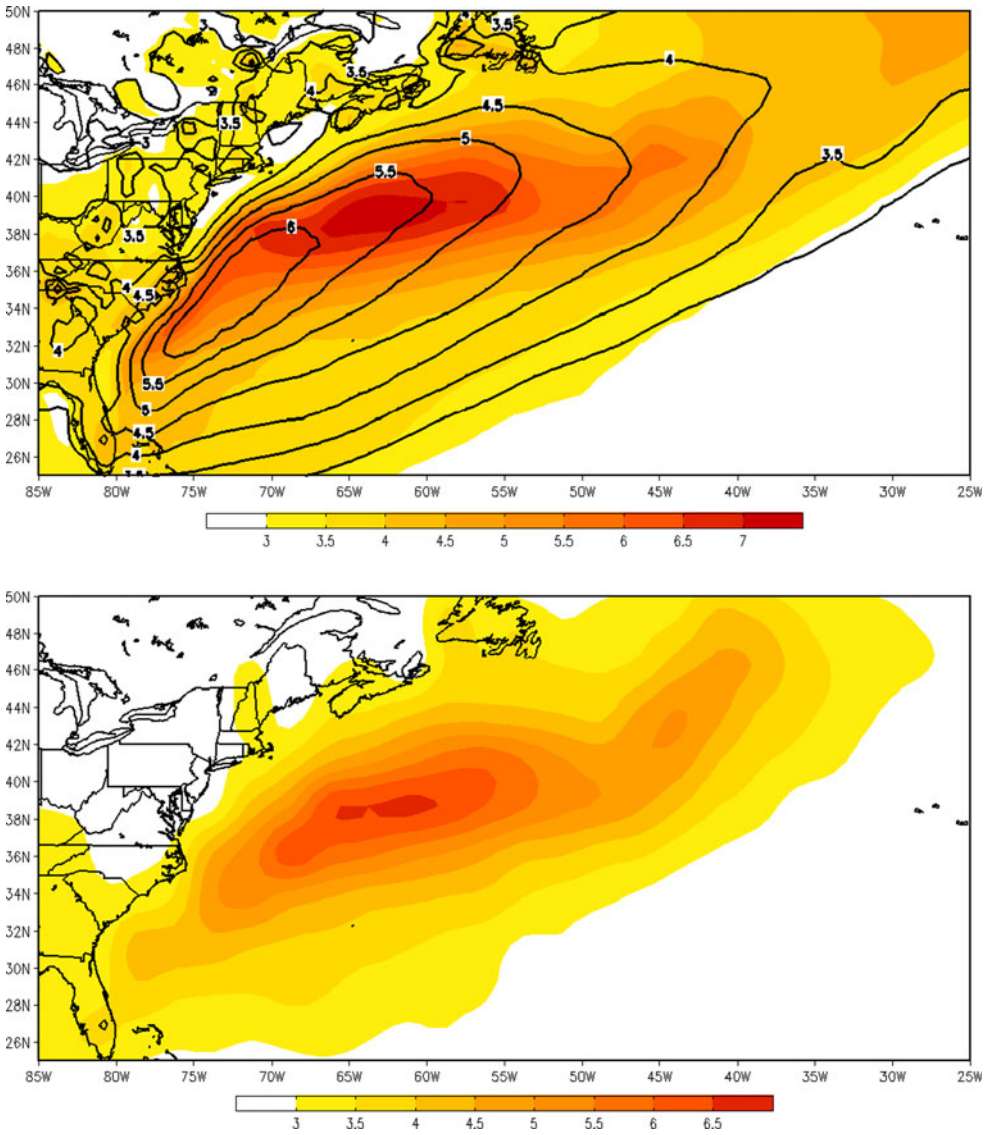

Fig. 8 The *top panel* shows the time mean precipitation in mm day^{-1} from LRC (*contours*) and HRC06 (*shaded*). The *bottom panel* shows climatological precipitation from observational estimates from Xie and Arkin (1997)

In order to examine the possible role of TIW, the near-equatorial (equator to 5°N) annual cycle of SST difference between HRC06 and LRC is shown in Fig. 11 (top panel). The HRC06 simulation is generally warmer than the LRC simulation throughout the year, but there is a notable increase in the relative warmth during the peak cold-tongue season (August through November) in the Pacific, which migrates westward through the early boreal winter. This peak cold tongue season is precisely when the TIW are preferentially excited. The warmer temperatures are consistent with enhanced rainfall (see Fig. 6), and there is likely a positive feedback. Ultimately, either the sea-ice mechanism (i.e., Chiang and Bitz 2005), relative warming in the Northern Hemisphere (i.e., Kang et al. 2008) or the relative warming north of the equator due to the TIW are consistent with the differences (HRC06-LRC) in the tropical Pacific mean climate. Moreover, the differences in the annual cycle of the rainfall (Fig. 11 bottom) indicate a complex response.

4.5 Ocean stratification

The increase in horizontal ocean resolution could also lead to changes in the ocean thermal structure. Here we focus separately on the near equatorial upper ocean (max depth of 636 m) and the zonally averaged ocean stratification to a depth of 2,500 m. Figure 12 shows the annual mean ocean temperature averaged from 1S to 1N to a depth of 636 m for HRC06 (top), LRC (middle) and the difference (bottom). In the main thermocline in the eastern Pacific the high resolution simulation has reduced stratification. This can easily be detected in the difference plot (Fig. 12 bottom) as a vertically oriented dipole structure with warmer (colder) temperatures below (above) the main thermocline

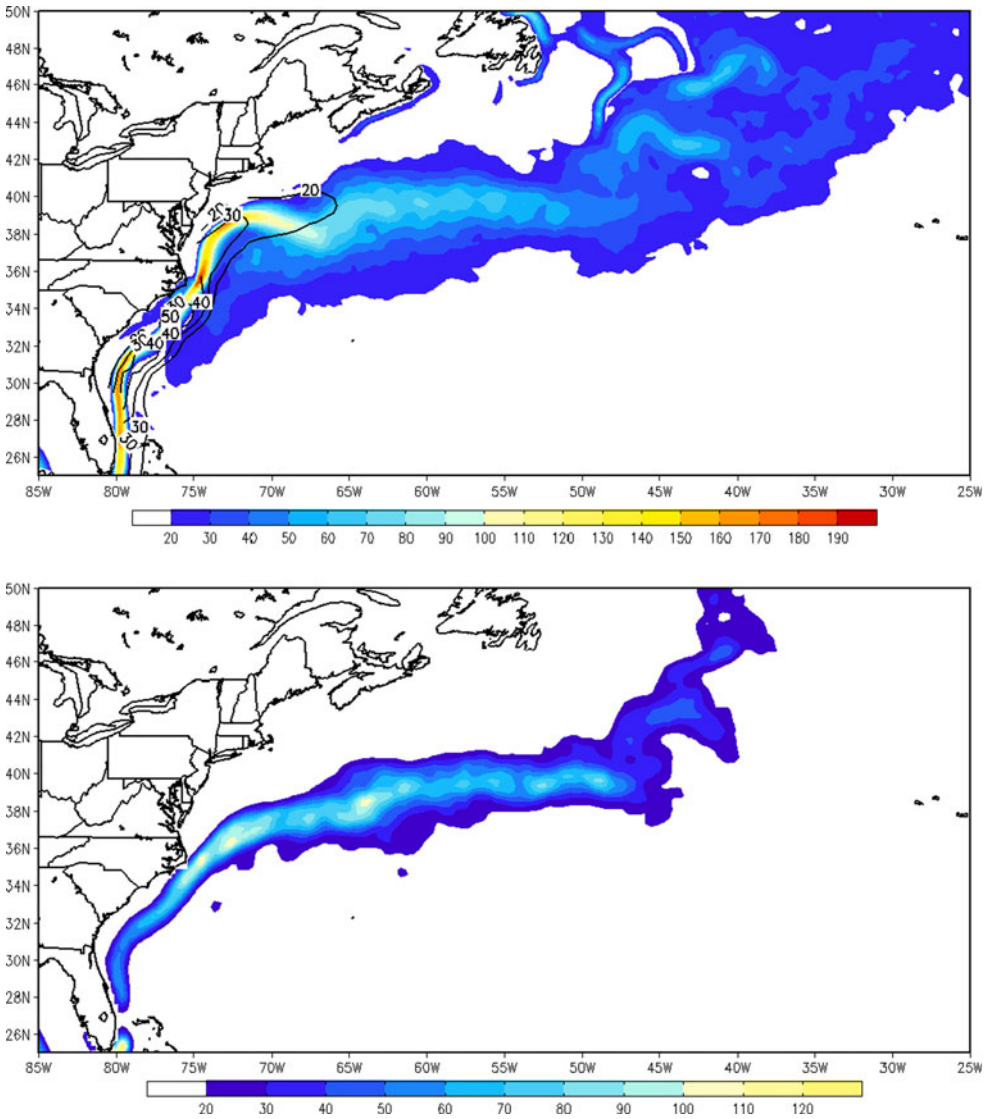

Fig. 9 The *top panel* shows the time mean surface current speeds in cm sec^{-1} from LRC (*contours*) and HRC06 (*shaded*). The *bottom panel* shows climatological surface currents from observational estimates from Maximenko and Hafner (2010)

in HRC06. The reduced eastern Pacific stratification can also be detected in the total fields (Fig. 12 top and middle). The western equatorial Atlantic also has reduced stratification in the HRC06 simulation. The changes in the Indian Ocean main thermocline stratification are more subtle. We argue that these changes in the stratification is due to the numeric at high resolution as opposed to the eddies themselves. The Pacific thermocline slope is also somewhat weaker in HRC06. This is also consistent with changes in the equatorial winds discussed in Sect. 7. Hecht (2010) show that the equatorial stratification (and subsurface current shears) are sensitive to choices of advection scheme in the eddy-resolving regime, and that the reduced stratification in the eastern Pacific may be the result of excessive spurious mixing resulting from inaccuracies in the advection scheme.

In a similar format as Fig. 12, the zonally averaged thermal structure is shown in Fig. 13 to a maximum depth of 2,500 m. At most latitudes and with a maximum in tropics and sub-tropics the deep ocean (below 1,000 m) is colder in HRC06 and is indicative of increased stratification below the main thermocline. Above 1,000 m at most latitude HRC06 is warmer than LRC. The maximum relative warming is poleward of 30 in both Hemispheres.

5 Sea-ice

The horizontal resolution of the sea-ice model is identical to the ocean model used in HRC06 and LRC, respectively. As a consequence, significant changes in the sea-ice climatology would be expected. Here we document the changes in the sea-ice for both the Arctic and the Antarctic at the two extremes of the annual cycle (i.e., March and September). The results for the Arctic are shown in Fig. 14 and include the sea-ice concentrations from HRC06 and

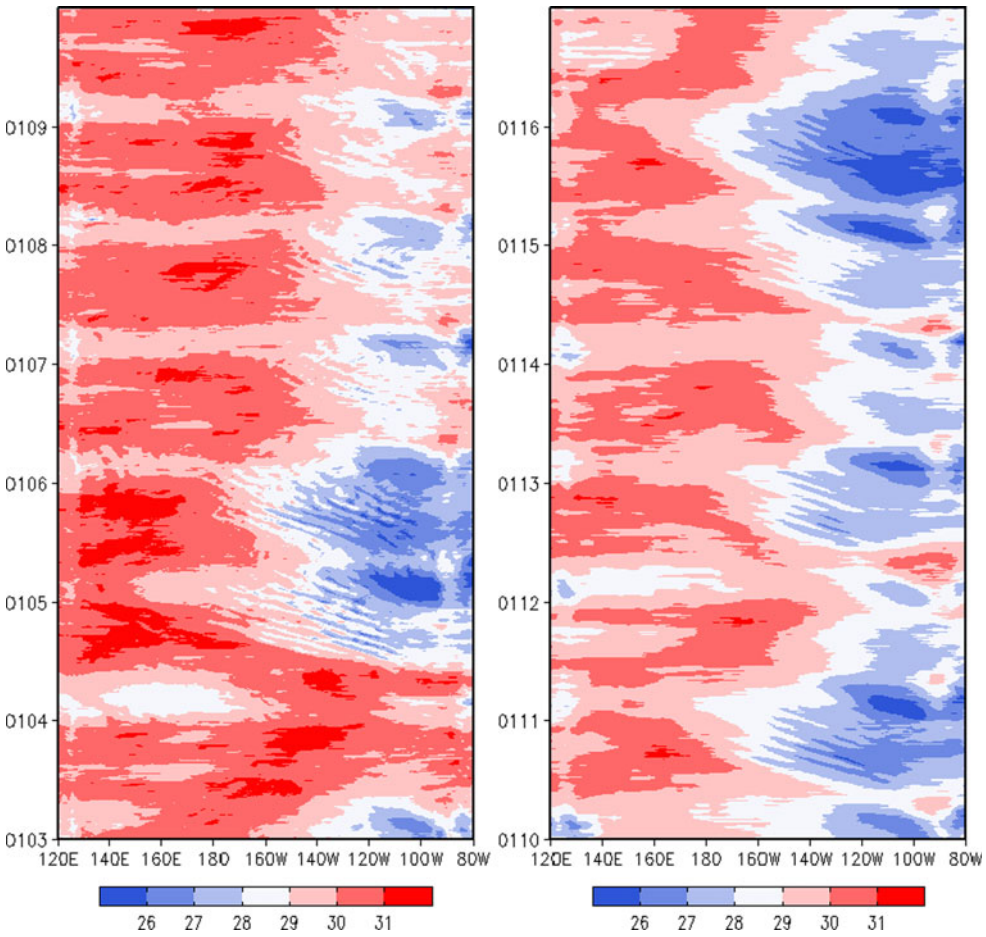

Fig. 10 Time-longitude sections of Pacific daily SST averaged from 3°N to 6°N for both HRC06 (*left panel*) and LRC (*right panel*) in °C

LRC. In the same format, the results for the Antarctic are plotted in Fig. 15. At both extremes, the Northern Hemisphere (Fig. 14 upper left and right) sea-ice area is considerably smaller in the HRC06 simulation compared to LRC. This relative decrease is most notable in March in the Nordic Seas extending into the Barents and Laptev Seas and in September in the central Arctic. In these regions LRC agrees more favorably with current sea ice observations (e.g., Comiso 1999). Sizable decreases are also seen in March in the Bering Sea and the Sea of Okhotsk.

A primary reason for the lack of sea ice in the Atlantic sector and central Arctic in HRC06 compared to LRC is the relatively higher ocean heat transport into the Nordic Seas and Arctic in HRC06. Interestingly, transport of the mean temperature by the mean currents is the key difference, rather than by eddies (see Sect. 6 below).

In the Southern Hemisphere, during both the annual minimum (March; Fig. 15 upper panels) and the annual maximum (September; Fig. 15 lower panels), the sea-ice concentrations are slightly smaller in the HRC06 simulation. Thus the relative reduction in the Southern Hemisphere is much less than in the Northern Hemisphere. In other words, the relative lack of Arctic sea-ice but comparable Antarctic sea ice in the HRC06 compared to LRC simulations is a striking hemispherically asymmetric difference between the two runs. The lack of Arctic sea ice occurs with strong Arctic warming that reaches all the way to the tropics in HRC06 compared to LRC and is consistent with the southward shift of the ITCZ in the tropical Pacific noted earlier (see also Chiang and Bitz 2005).

6 Understanding the warming signal

The intent of this section is to document some of the sources of the warming signal seen in HRC06 compared to LRC. There are several elements to the warming:

First, there is a significant increase in the poleward ocean heat transport in HRC06, which is largely due to changes in the mean as opposed to the eddy transport. For example, Fig. 16 shows the global northward ocean heat transport for HRC06 (red curves) and LRC (blue curves). The heat transports have been separated into eddy (dot-dashed curves) and mean (dashed curves) terms. The observational estimate of Trenberth and Caron (2001) is shown for comparison. At all latitudes in the Northern

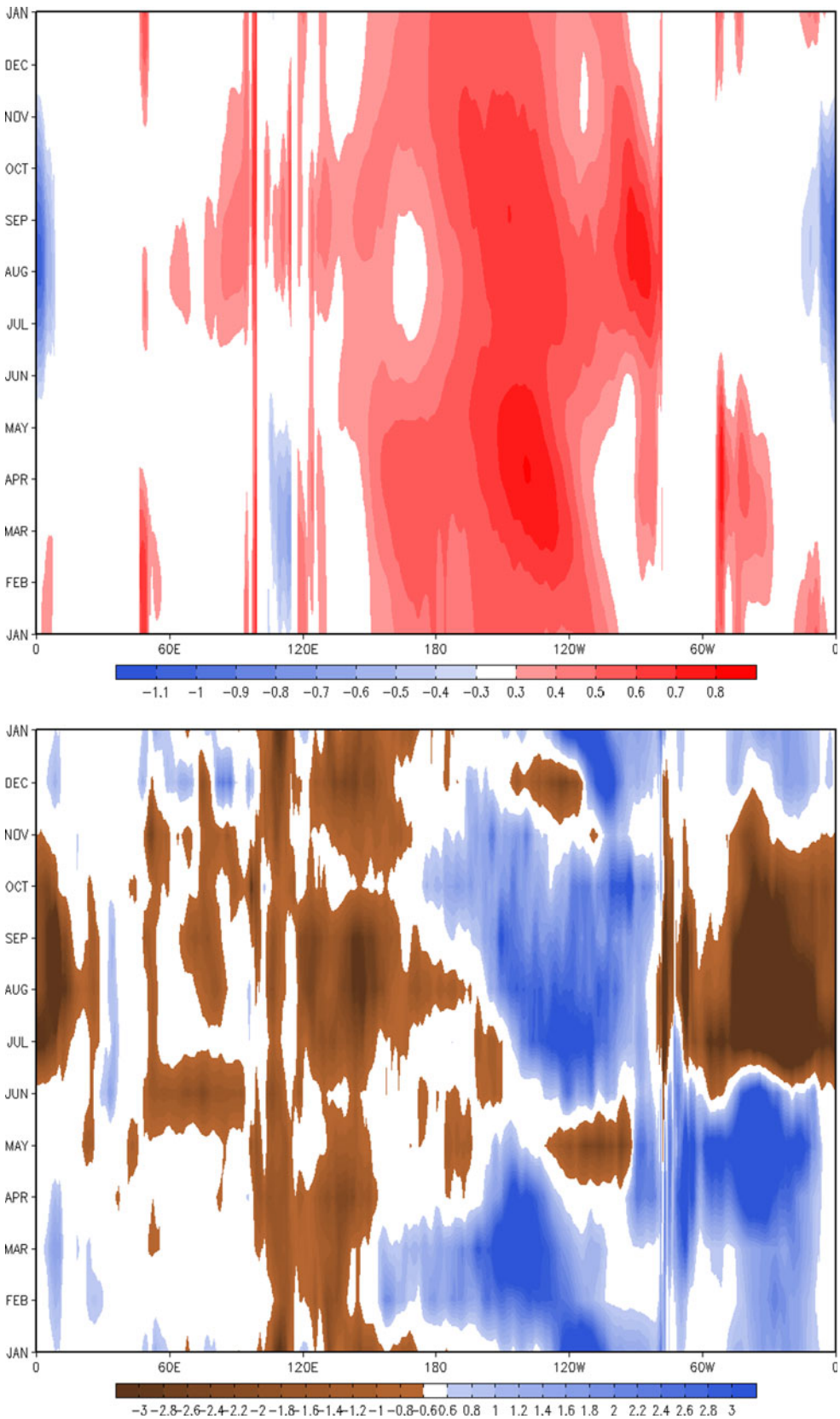

Fig. 11 (*Top*) Difference (HRC06-LRC) in the time-longitude evolution of the mean annual cycle of SST averaged from 3 to 6 N in degrees Celsius. (*Bottom*) Difference (HRC06-LRC) in the time-longitude evolution of the mean annual cycle of precipitation averaged from 3 to 6 N in mm day^{-1}

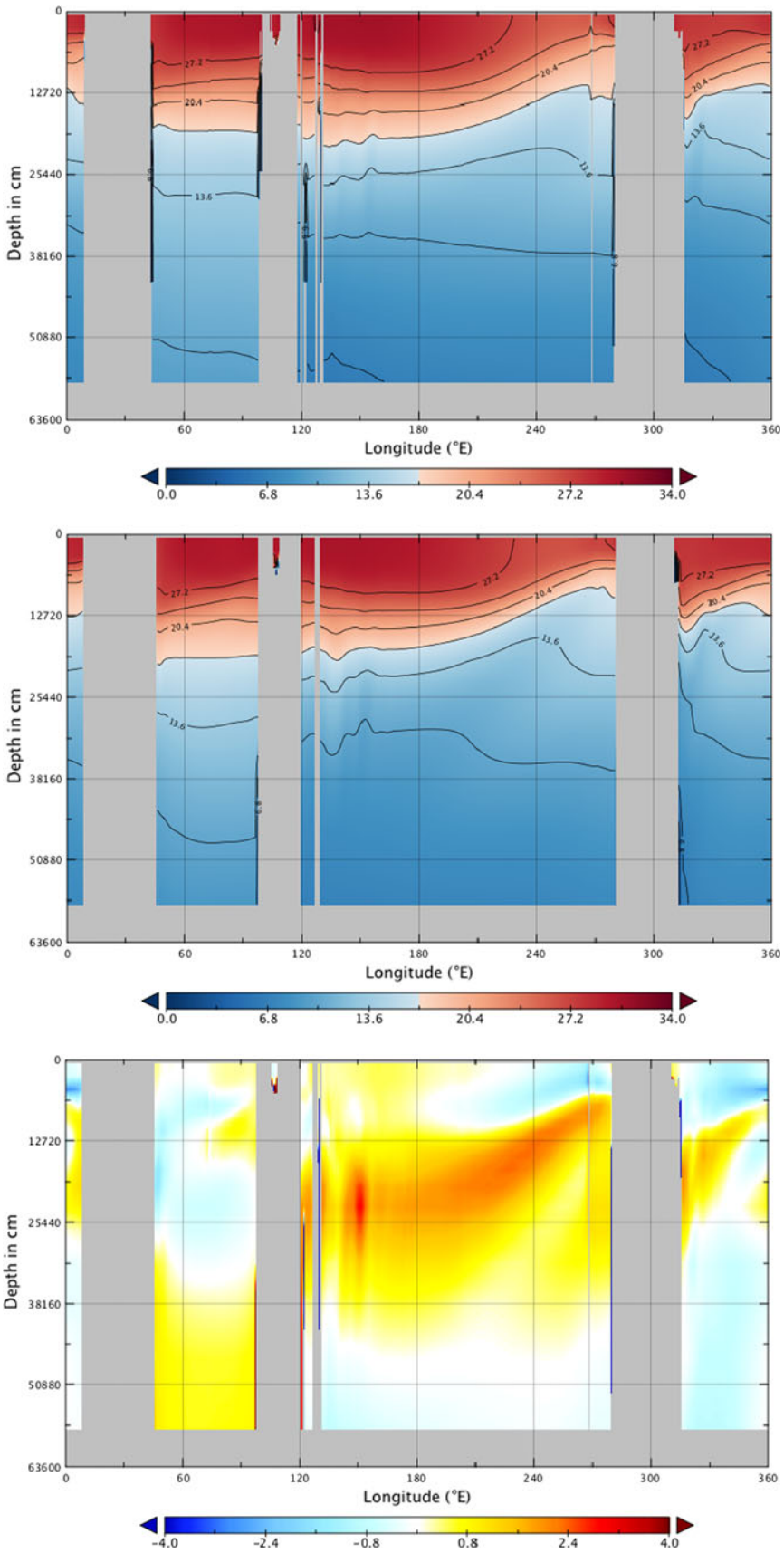

Fig. 12 Time mean vertical structure of upper Ocean equatorial temperature averaged between 1S and 1 N in HRC06 (*top*) and LRC (*middle*) and HRC06-LRC (*bottom*) in degrees Celsius. Maximum depth in all panels is 636 m

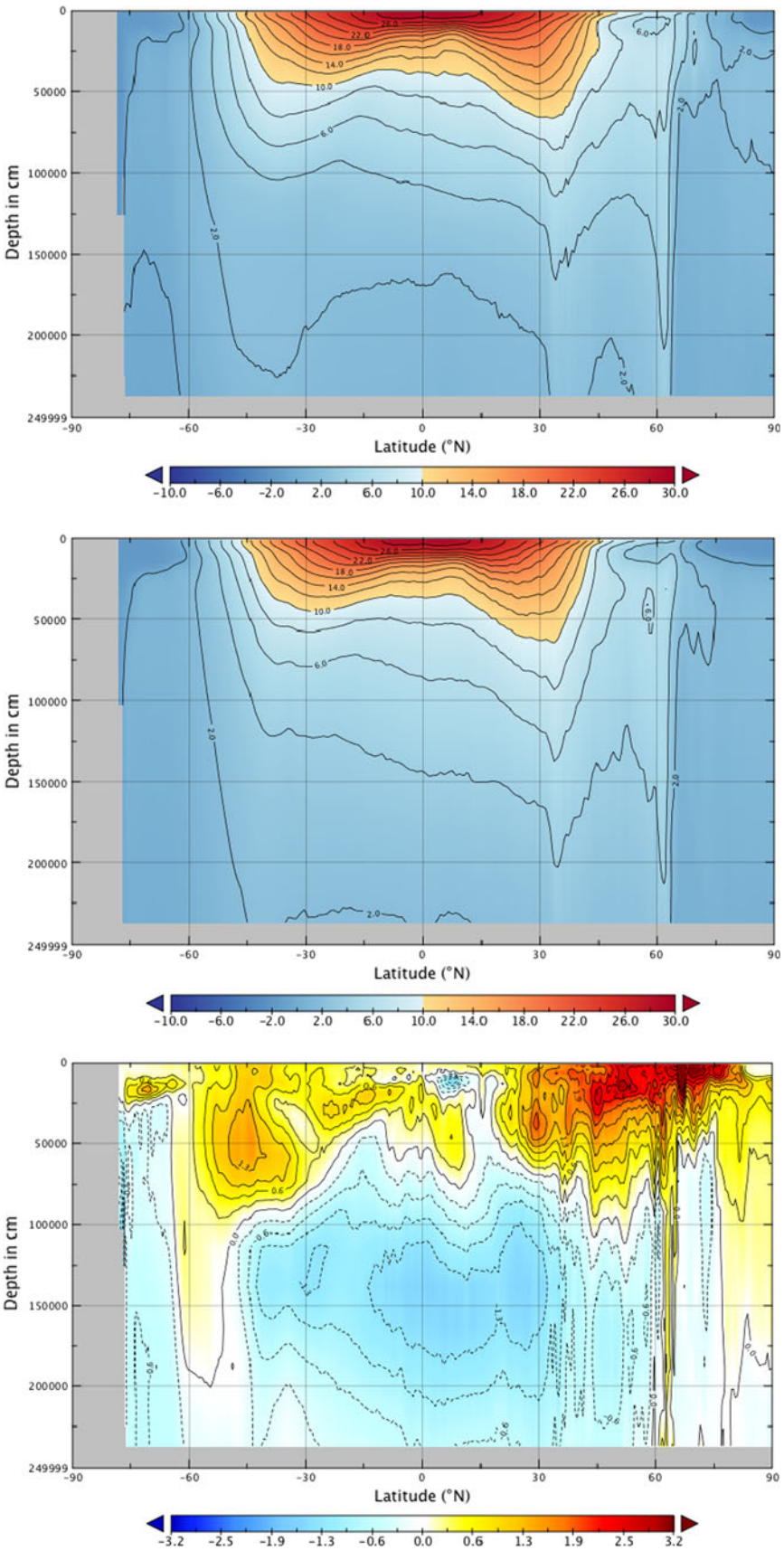

Fig. 13 Time mean vertical structure zonally averaged temperature HRC06 (*top*) and LRC (*middle*) and HRC06-LRC (*bottom*) in degrees Celsius. Maximum depth on all three panels is 2,500 m

Hemisphere the northward heat flux is larger in HRC06 and poleward of 50 N the eddy transports are negligible compared to the mean transport. Additional analysis indicates that the ocean heat transport between 60 N and 80 N in the high-resolution simulation is dominated by the Norwegian current. The Norwegian current extension of the North Atlantic current is unresolved and undetected in the low-resolution simulation, and it is the ocean heat transport associated with this current system that initiates the sea-ice loss in the high-resolution simulation.

Second, this enhanced poleward heat transport is associated with large reductions in Northern Hemisphere sea-ice (Fig. 14). An ice-albedo feedback, in turn, leads to even further polar warming. For instance, Fig. 17 (top) shows the climatological difference (HRC06-LRC) in the short wave radiation absorbed at surface. In the reduced sea-ice polar regions the increase in short wave radiation absorbed at the surface is on the order of 20–25 W m^{-2}.

Third, there is enhanced warming in the North Pacific and North Atlantic in the central basin to the east of the

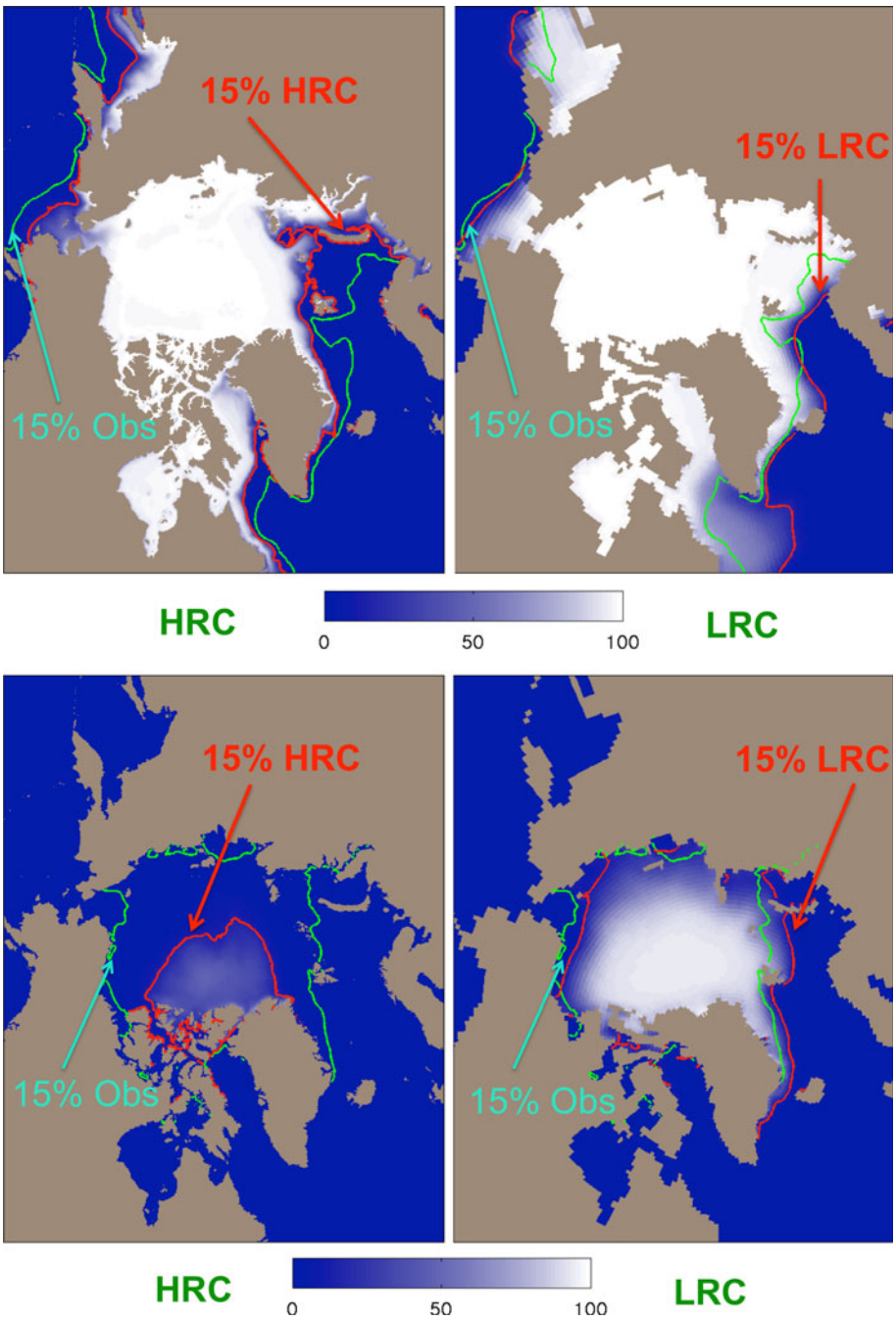

Fig. 14 Arctic sea ice concentration in March (*upper panels*) and September (*lower panels*) for HRC and LRC runs. The 15 % concentration contour from the model is shown in red and from observations in green. Observations are from passive microwave averaged 1979–1999 (Comiso 1999)

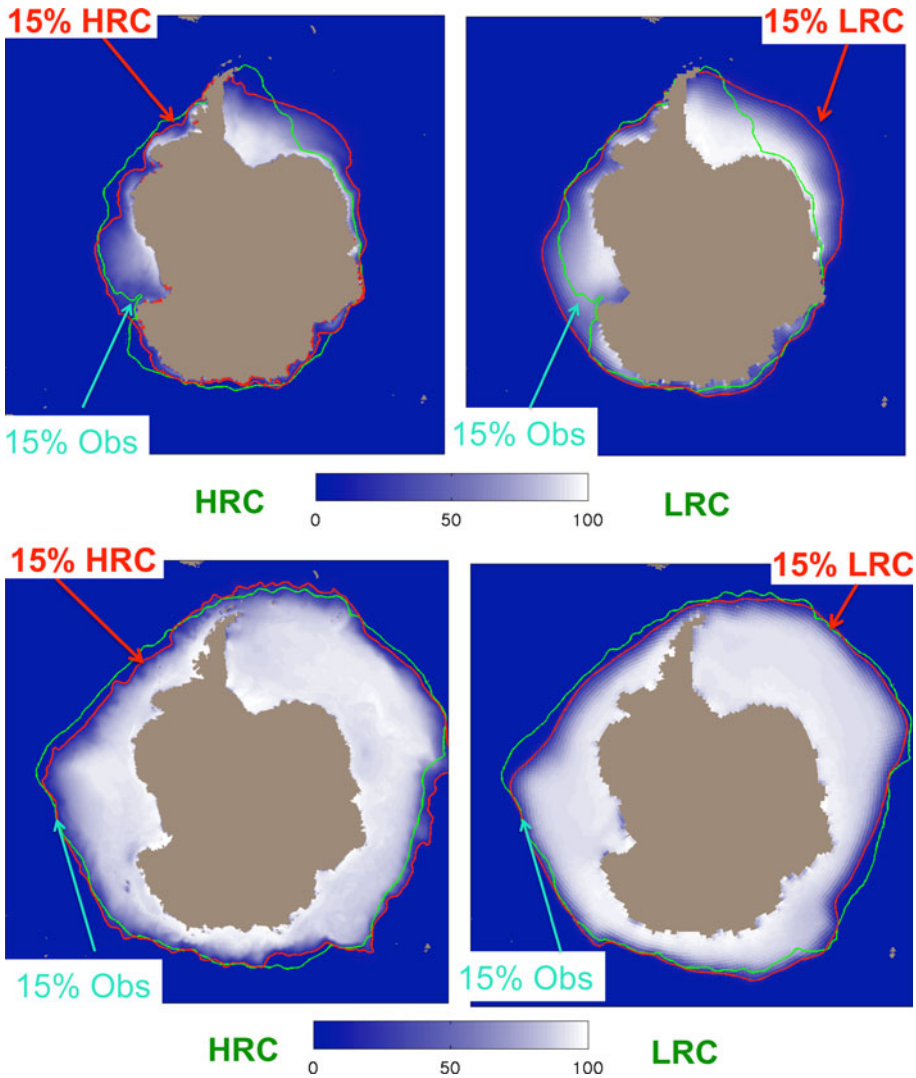

Fig. 15 As for Fig. 14, but for Antarctic

major western boundary currents. This increase is associated with the increase in short wave radiation absorbed seen above. At first this is somewhat surprising since there are increases in rainfall in these regions as shown in Fig. 6 (top) and expected increases in cloud cover. The change in solar radiation at the surface is driven by changes in types of cloud cover. For instance, in LRC there are ubiquitous low clouds that serve to increase the albedo relative to HRC06. HRC06 has more precipitating clouds, which serves to suppress the ubiquitous low cloud, ultimately leading to an increase in solar radiation absorbed at the sea surface seen in Fig. 17 (top).

Fourth, most of the sub-tropics and tropics show a decrease in short wave radiation absorbed at the surface except in regions where there are large decreases in tropical rainfall and cloud cover (in this case there is little compensating increase in low cloud). The warming in the tropics and sub-tropics appears to be largely a long-wave radiation—increased water vapor greenhouse feedback. This can be seen in Fig. 17 (bottom) where we have plotted

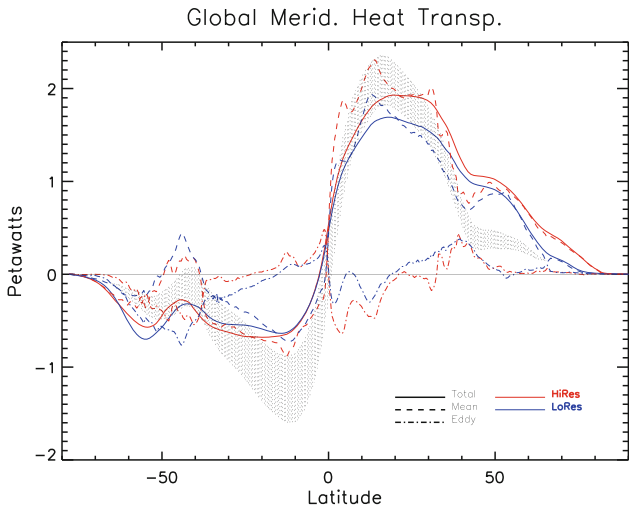

Fig. 16 Global northward meridional heat transport. HRC06 results are in *red* and LRC results are in *blue*. The *solid curves* give the total transport, the *dashed curves* give the mean transport and the *dot-dashed curves* give the eddy transport. The observed estimates are from Trenberth and Caron (2001) and units are in petawatts

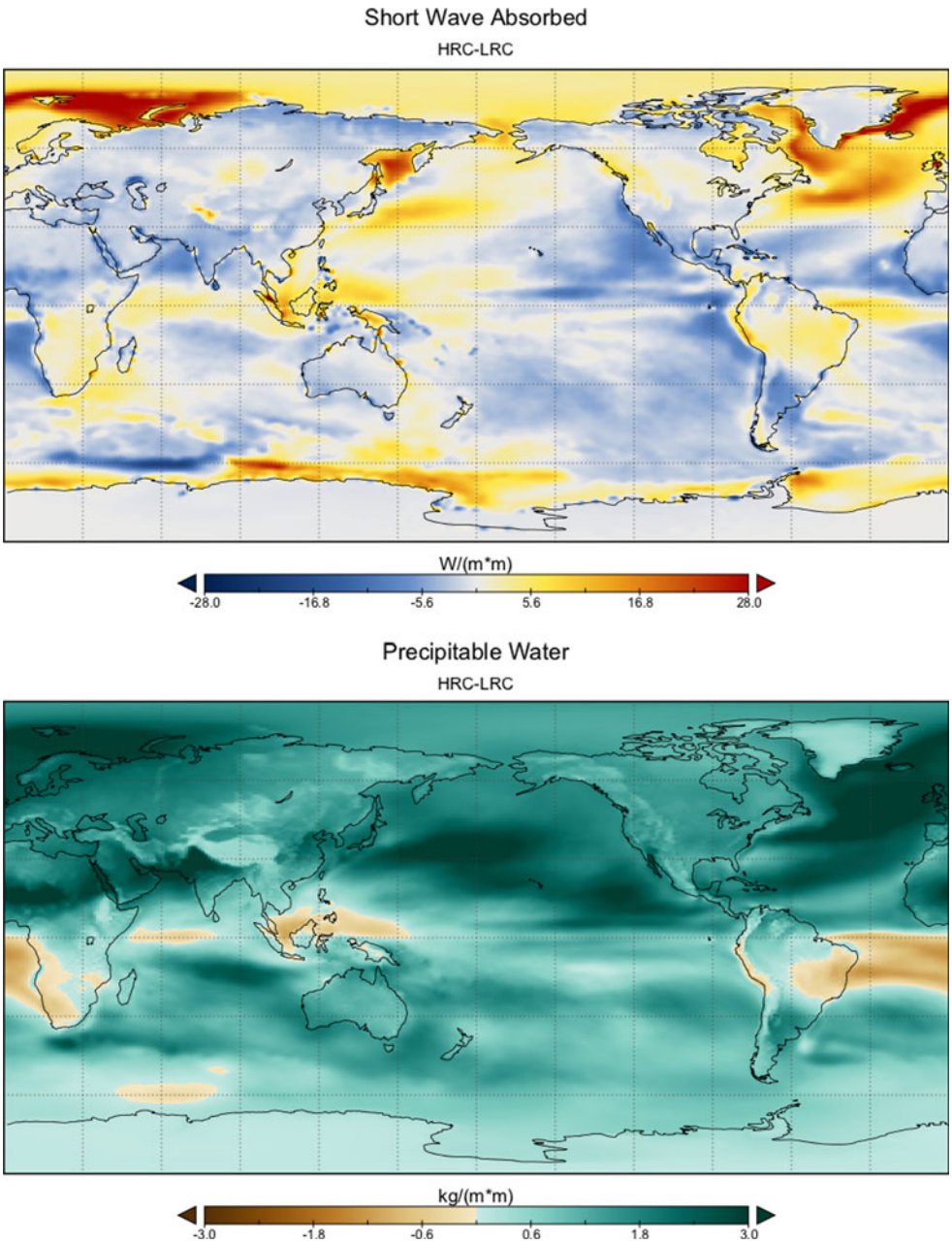

Fig. 17 The *top panel* shows the time mean difference (HRC06-LRC) in short wave radiation absorbed at the surface in Watts m^{-2}. The *bottom panel* shows the time mean difference (HRC06-LRC) in precipitable water in kg m^{-2}

the climatological difference (HRC06-LRC) in precipitable water. The increase in precipitable water occurs everywhere expect in tropical regions where we noted relatively large decreases in rainfall.

7 Interannual variability

An important question is how higher ocean model resolution impacts the seasonal-to-interannual variability. In this respect, we concentrate on the variability of monthly mean SST anomalies (SSTA). Figure 18 (top), for example, shows the ratio of the SSTA monthly standard deviation for HRC06 compared to LRC. The standard deviation is calculated on the atmospheric model grid. The SST variability applied to the atmosphere is clearly enhanced in HRC06 throughout most of the mid-latitudes and the subtropics. The core regions of substantially enhanced variance include the Northern Hemisphere western boundary current zones and the Southern Ocean from the Atlantic coast of South America extending through to the Pacific side of the Australian continent. The enhanced variance in these regions is arguably expected given the enhanced eddy activity in HRC06, and later we show evidence that the enhance variability is, in fact, interacting with the atmosphere.

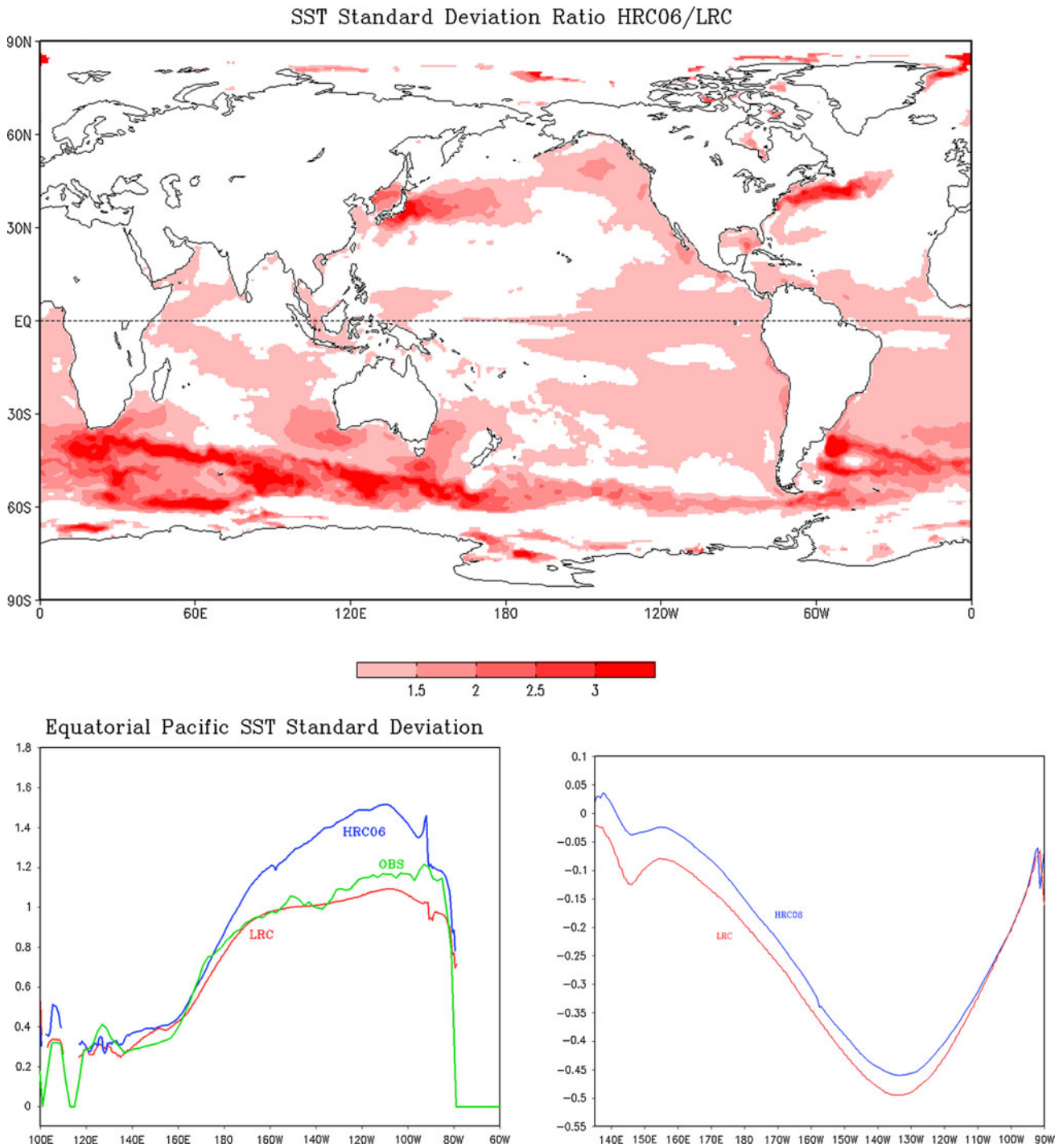

Fig. 18 (*Top*) SSTA monthly mean standard deviation ratio (HRC06/LRC)—dimensionless. Values greater than 1.0 indicate more variance in HRC06 and only plotted when statistically significant at the 99 % confidence interval. (*Bottom left*) SSTA monthly mean standard deviation near the equator (1S–1 N) in the Pacific for LRC (*red*) and HRC06 (*blue*) in degrees Celsius. Observational estimates are given in *green*. (*Bottom right*) Time mean zonal wind stress in dyn cm^{-2} near the equator (1S–1 N) in the Pacific for LRC (*red*) and HRC06 (*blue*)

There are also relatively small, but statistically significant increases in variance in the tropics. The increases in the tropics contrast the extra-tropics in that the character of the variance changes does not show the signature of enhanced eddy activity. Indeed, the increase in tropical variance is largely ascribed to the increase in ENSO variance (see Fig. 18 lower left). On the one hand, the changes in stratification (i.e., relatively weaker equatorial

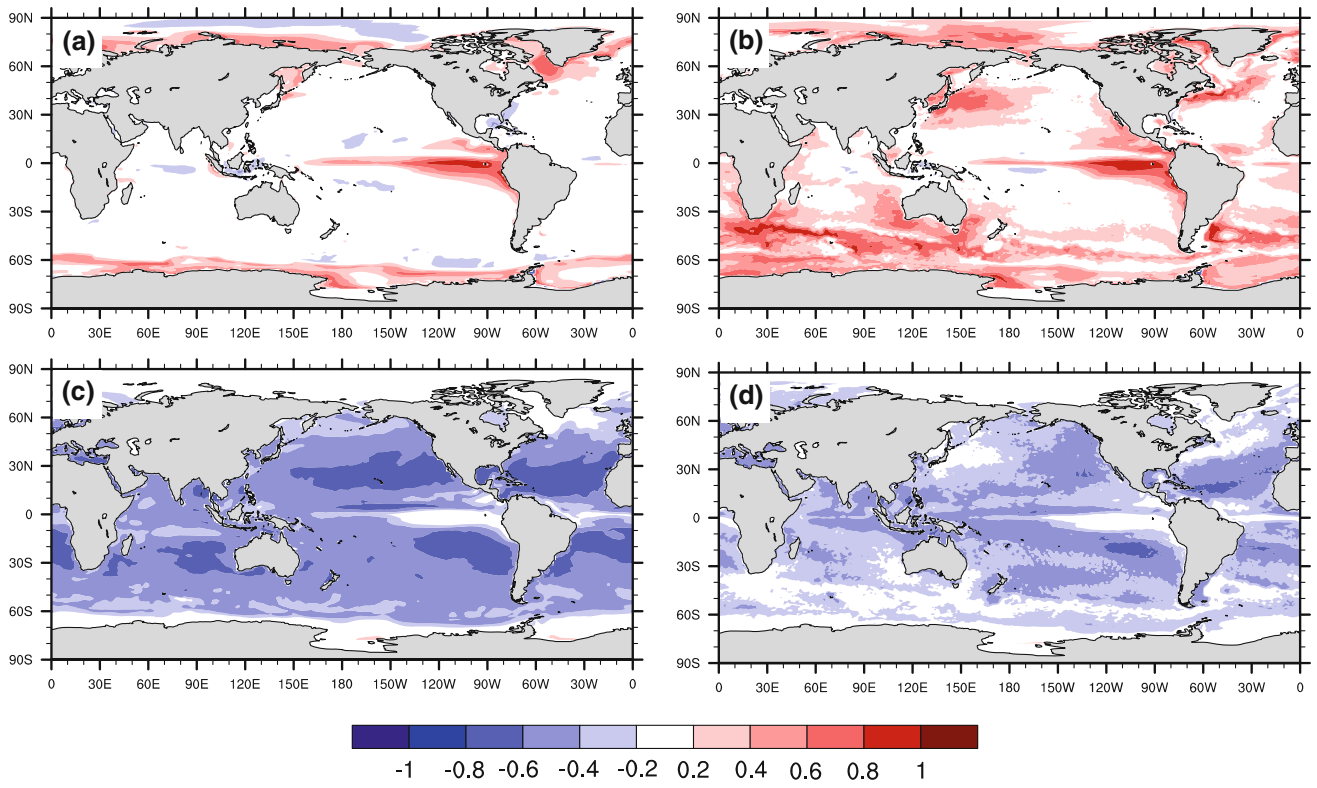

Fig. 19 Simultaneous pointwise correlations between turbulent heat flux (sensible +latent) and SST, **a** low-resolution, **b** high-resolution, and between turbulent heat flux and SST tendency, **c** low-resolution, **d** high-resolution. All calculations were done using monthly averages, with the least squares trend and monthly climatology subtracted. The SST tendency was calculated by center differencing over 2 months

stratification) with HRC06 would suggest decreased ENSO variance (see Meehl et al. 2001). On the other hand, the equatorial Pacific easterlies are generally weaker in HRC06 relative to LRC (see Fig. 18 lower right). The weaker easterlies are consistent with stronger ENSO variance (e.g., Kirtman and Schopf 1998; Burgman et al. 2008). In the absence of any subsurface stratification changes Kirtman and Schopf (1998) found that a decrease in the surface easterlies on the order of 0.025 dynes cm^{-2} lead to an increase of ENSO variance by about a factor of 2. Here we find larger reductions in the easterlies and smaller increases in ENSO variance. Presumably the smaller increase in ENSO variance is due to the compensating effect of the reduced equatorial Pacific stratification.

To examine the changes in air-sea feedbacks with ocean resolution we have adopted the methodology first suggested by Barsugli and Battisti (1998) and von Storch (2000) that was later applied to coupled models by Kirtman and Vecchi (2010), Wu and Kirtman (2007), Wu et al. (2007) and Wu et al. (2006). These papers argue that, to first order, when the local point-by-point simultaneous correlation between the surface heat flux and the SSTA is strongly positive (with the sign convention that the heat flux is positive upward—from ocean to atmosphere), the SST variability can be viewed as forcing the atmosphere. Conversely, when atmospheric forcing of SST variability dominates, there is a stronger (negative) simultaneous correlation between the surface flux and SST tendency, and the simultaneous correlation between heat flux and SSTA tends to be small. The simultaneous local correlations of SSTA and SSTA tendency with surface turbulent heat flux (latent plus sensible) are shown in Fig. 19 for the two models, indicating significant differences, especially at mid-latitudes. The regions of enhanced SST variability in the Kuroshio, Gulf Stream and Antarctic Circumpolar Current in HRC06 apparent in Fig. 18 all show strong positive correlations between SSTA and surface heat flux (Fig. 19b). The SST variability in these regions is strongly related to the variability associated with the better-resolved currents and eddies. With the exception of the ENSO signature in the tropical Pacific, the correlation between SSTA and surface flux is small in LRC (Fig. 19a). The correlation between surface flux and SST tendency is strongly negative over most of the ocean in LRC (Fig. 19c), an indication of the predominance of atmospheric forcing of SST variability at this resolution. For HRC06, the correlation between SST tendency and surface flux remains negative, but weaker than in LRC, over most of the ocean (Fig. 19d) with holes in those regions where ocean dynamics contribute strongly to SST variability. In addition to the

western boundary current systems and ACC region stronger SST forcing of the atmosphere is evident in HRC06 along the west coasts of North and South America, Australia, and southern Africa.

As noted in Sect. 3, mean precipitation and SST differences are consistent with one another in that regions of enhanced mean mid-latitude rainfall coincide with large positive temperature differences associated with the western boundary currents. Some of the enhanced mean rainfall in these regions may also be the result of greater *temporal SST variability* along with stronger coupling between the SST variability and latent heat flux—with the ocean forcing the atmosphere—in the HRC06 compared to LRC simulation. When the ocean is driving an atmospheric response, a warm SST anomaly is associated with a larger increase in latent heat flux than the decrease in latent heat flux associated with a cold SST anomaly of the same magnitude because of the non-linear relationship between temperature and saturation vapor pressure. The result is a net mean increase in the flux of moisture into the atmosphere in the HRC06 simulation. A similar argument applies to stationary, spatial variability in the SST fields. In the tropics, the differences between HRC06 and LRC are relatively small as expected from the differences in the SSTA variance.

8 Summary and concluding remarks

The objective of the numerical experiments presented here was to examine how resolved ocean fronts and eddies impact the large-scale climate. To do this we examined two simulations of CCSM3.5. In the first simulation (LRC) the 0.5° atmosphere and land-surface components were coupled to ocean and sea-ice components with zonal resolution of 1.2° and meridional resolution varying from 0.27° at the equator to 0.54° in the mid-latitudes. In the ocean eddy resolving simulation (HRC06), the same atmosphere and land-surface models were coupled to ocean and sea-ice components with 0.1° resolution globally. The results described here present an overall view of the simulations, and serve to encourage more detailed studies. There are some notable climatic impacts, for example:

1. The high-resolution simulation is ubiquitously warmer than the low-resolution simulation. The largest differences are in the Arctic with notable losses of sea-ice and in regions of relatively large ocean eddy activity (i.e., Southern Ocean and western boundary currents). The loss of sea-ice appears to be due to increase mean northward ocean heat transport. Surprisingly, this increase in heat transport is not due to eddies, but is due changes in the mean circulation. The ubiquitous warming involves an ice-albedo feedback in the polar latitudes, changes in cloud cover in the western boundary current regions and global water vapor in the tropics and sub-tropics.
2. The SST front associated with the Gulf Stream is better resolved in the high-resolution simulation. This leads to large structural changes in the mean rainfall. Similar changes in the currents are seen in the vicinity of the Kuroshio, but the increased ocean resolution is apparently not as important for maintaining the SST gradient, as the temperature and rainfall differences are small compared to the Gulf Stream.
3. The equatorial stratification in the main thermocline (upper 500 m) of the Pacific and Atlantic Oceans weakens with the inclusion of resolved eddies. Conversely, the deep ocean (below 1,000 m) stratification increases at all latitudes.
4. The variability of monthly mean SSTA increases with increasing ocean resolution throughout the extra-tropics. This increase is most notable in the western boundary current regions and the Southern Ocean. The variance increased in the tropics also, but this change is apparently linked to an increase in ENSO variance as opposed to a direct affect of the resolved eddies.
5. There were notable differences in local air-sea interactions. In the extra-tropics there is evidence of stronger forcing of the atmosphere by SST variability arising from ocean dynamics. In fact, in the lower resolution simulation, the coupling between SSTA and surface heat flux is very weak.

Finally we note that we focused on how the resolved eddies impact simulation without any changes to the parameterizations—we take it for granted that significant effort is still required to ensure that the model with increased resolution can be further refined to produce improved simulations. In fact, we hope these simulations can be used to guide such an effort.

Acknowledgments We acknowledge the support of the National Science Foundation (J. Kinter and C Stan through AGS 0830068 and OCI 0749290; B. Kirtman through OCI 0749165, AGS 0754341 and AGS 0850897; C. Bitz through ARC 0938204; F. Bryan, J. Dennis, N. Hearn, R. Loft, R. Tomas and M. Vertenstein through its support of NCAR). B. Kirtman also acknowledges support from the NOAA NA08OAR3420889. Computing resources were provided by the National Institute of Computational Sciences at the University of Tennessee through an award made by the TeraGrid Resource Allocations Committee.

References

An S-I (2008) Interannual variations of the tropical instability wave and ENSO. J Climate 21:3680–3685. doi:10.1175/2008JCLI1701.1

Barsugli JJ, Battisti DS (1998) The basic effects of atmosphere-ocean thermal coupling on midlatitude variability. J Atmos Sci 55: 477–493

Brankovic C, Gregory D (2001) Impact of horizontal resolution on seasonal integrations. Clim Dyn 18:123–143. doi:10.1007/s003820100165

Brunet G et al (2010) Collaboration of the weather and climate communities to advance subseasonal-to-seasonal prediction. Bull Am Meteor Soc 91:1397–1406

Bryan FO, Hecht MW, Smith RD (2007) Resolution convergence and sensitivity studies with North Atlantic ciculation models. Part I: the western boundary current system. Ocean Model 16:141–159

Bryan FO, Tomas R, Dennis JM, Chelton DB, Loeb NG, McClean JL (2010) Frontal scale air–sea interaction in high-resolution coupled climate models. J Climate 23:6277–6291. doi:10.1175/2010JCLI3665.1

Burgman RJ, Schopf PS, Kirtman BP (2008) ENSO decadal variability. J Climate 21:5482–5550

Casey KS, Brandon TB, Cornillon P, Evans R (2010) The past, present and future of the AVHRR pathfinder SST program. In: Barale V, Gower JFR, Alberotanza L (eds) Oceanography from space: revisited. Springer, Berlin. doi:10.1007/978-90-481-8681-5_16

Chelton DB, Esbensen SK, Schlax MG, Thum N, Freilich MH, Wentz FJ, Gentemann CL, McPhaden MJ, Schopf PS (2001) observations of coupling between surface wind stress and sea surface temperature in the eastern Tropical Pacific. J Climate 4: 1479–1498

Chiang JCH, Bitz CM (2005) Influence of high latitude ice cover on the marine intertropical convergence zone. Clim Dyn. doi:10.1007/s00382-005-0040-5

Comiso J (1999) updated 2008./Bootstrap sea ice concentrations from Nimbus-7 SMMR and DMSP SSM/I/. National Snow and Ice Data Center, Digital media, Boulder, CO

Craig AP, Jacob R, Kauffman B, Bettge T, Larson J, Ong E, Ding C, He Y (2005) CPL6: the new extensible, high performance parallel coupler for the community climate system model. High Perf Comp Appl 19:309–328

Craig A, Vertenstein M, Jacob R (2011) A new flexible coupler for earth system modeling developed for CESM4 and CESM1. Int J High Perf Comput Appl 26:31–42. doi:10.1177/1094342011428141

Delworth TL, Rosati A, Anderson W, Adcroft AJ, Balaji V, Benson R, Dixon K, Griffies SM, Lee H-C, Pacanowski RC, Vecchi GA, Wittenberg AT, Zeng F, Zhang R (2012) Simulated climate and climate change in the GFDL CM2.5 high-resolution coupled climate model. J Climate 25:2755–2781. doi: 10.1175/Jcli-D-11-00316.1

Dennis JM, Vertenstein M, Worley P, Mirin A, Craig A, Jacob R, Mickelson S (2012) Computational performance of ultra-high resolution capability in the community earth system model. Int J High Perf Comput Appl 26:5–16. doi: 10.1177/1094342012436965

Deser C, Tomas R, Alexander M, Lawrence D (2010) The seasonal atmospheric response to projected arctic sea ice loss in the late twenty-first century. J Climate 23:333–351. doi:10.1175/2009JCLI3053.1

Gent PR, Yeager SG, Neale RB, Levis S, Bailey DA (2010) Improvements in a half degree atmosphere/land version of the CCSM. Clim Dyn 34:819–833

Hack JJ, Caron JM, Danabasoglu G, Oleson KW, Bitz C, Truesdale JE (2006) CCSM–CAM3 climate simulation sensitivity to changes in horizontal resolution. J Climate 19:2267–2289. doi:10.1175/JCLI3764.1

Hecht MW (2010) Cautionary tales of persistent accumulation of numerical error: dispersive centered advection. Ocean Model 35:270–276. doi:10.1016/J.Ocemod.2010.07.005

Hurrell J, Meehl GA, Bader D, Delworth TL, Kirtman B, Wielicki B (2009) A unified modeling approach to climate system prediction. Bull Am Meteor Soc 90:1819–1832

Jochum M, Murtugudde R (2004) Internal variability of the tropical Pacific Ocean. Geo Phys Res Lett 31:L14309

Jochum M, Desser C, Phillips A (2007) Tropical atmospheric variability forced by oceanic internal variability. J Climate 20: 765–771

Jochum M, Danabasoglu G, Holland MM, Kwon YO, Large WG (2008) Ocean viscosity and climate. J Geophys Res 113. doi:10.1029/2007JC004515

Kalnay E et al (1996) The NCEP/NCAR 40-year reanalysis project. Bull Am Meteor Soc 77:437–471

Kang SM, Held IM et al (2008) The response of the ITCZ to extratropical thermal forcing:idealized slab-ocean experiments with a GCM. J Climate 21(14):3521–3532

Kirtman BP, Schopf PS (1998) Decadal variability in ENSO predictability and prediction. J Climate 11:2804–2822

Kirtman BP, Vecchi G (2010) Why climate modelers should worry about the weather. In: Chang CP, Ding Y, Lau N-C, Johnson RH, Wang B, Yasunari T (eds) The global monsoon system: research and forecast, 2nd ed. World Scientific, Singapore, pp 511–523

Kobayashi C, Sugi M (2004) Impact of horizontal resolution on the simulation of the Asian summer monsoon and tropical cyclones in the JMA global model. Clim Dyn 23:165–176. doi:10.1007/s00382-004-0427-8

Kumar A, Perlwitz J, Eischeid J, Quan X, Xu T, Zhang T, Hoerling M, Jha B, Wang W (2010) Contribution of sea ice loss to Arctic amplification. Geophys Res Lett 37:L21701. doi:10.1029/2010GL045022

Lin S-J, Rood RB (1997) An explicit flux-form semi-Lagrangian shallow water model on the sphere. Q J R Meterol Soc 123: 2477–2498

Luo J-J, Masson S, Roeckner E, Madec G, Yamagata T (2005) Reducing climatology bias in an ocean-atmosphere OGCM with improved coupling physics. J Climate 18:2344–2360

Maloney ED, Chelton DB (2006) An assessment of sea surface temperature influence on surface winds in numerical weather prediction and climate models. J Climate 19:2743–2762

Maltrud M, Bryan F, Peacock S (2010) Boundary impulse response functions in a century-long eddying global ocean simulation. Environ Fluid Mech 10:275–295. doi:10.1007/s10652-009-9154-3

Maximenko NA, Hafner J (2010) SCUD: Surface CUrrents from Diagnostic model. IPRC Tech. Note 5, 17 pp. http://iprc.soest.hawaii.edu/publications/tech_notes.php

May W, Roeckner E (2001) A time-slice experiment with the ECHAM4 AGCM at high resolution: the impact of horizontal resolution on annual mean climate change. Clim Dyn 17:407–420. doi:10.1007/s003820000112

McClean JL, Bader DC, Bryan FO, Maltrud ME, Dennis JM, Mirin AA, Jones PW, Kim YY, Ivanova DP, Vertenstein M, Boyle JS, Jacob RL, Norton N, Craig A, Worley PH (2011) A prototype two-decade fully-coupled fine-resolution CCSM simulation. Ocean Model 39:10–30

Meehl GA et al (2001) Factors that affect the amplitude of El Nino in global coupled climate models. Clim Dyn 17:515–526

Minobe S, Kuwano A, Yoshida N, Komori S, Xie P, Small RJ (2008) Influence of the Gulf Stream on the troposphere. Science 452. doi:10.1038/Nature06690

Murray R (1996) Explicit generation of orthogonal grids for ocean models. J Comp Phys 126:251–273

Nakamura M, Enomoto T, Yamane S (2005) A simulation study of the 2003 heatwave in Europe. J Earth Simulator 2:55–69

Navarra A et al (2008) Atmospheric horizontal resolution affects tropical climate variability in coupled models. J Climate 21:730–750. doi:10.1175/2007JCLI1406.1

Neale RB, Richter JH, Jochum M (2008) The impact of convection on ENSO: from a delayed oscillator to a series of events. J Climate 21:5904–5924

Pope V, Stratton R (2002) The processes governing horizontal resolution sensitivity in a climate model. Clim Dyn 19:211–236. doi:10.1007/s00382-001-0222-8

Randall DA, Khairoutdinov M, Arakawa A, Grabowski W (2003) Breaking the cloud-parameterization dead- lock. Bull Am Meteor Soc 84:1547–1564

Roberts MJ, Clayton A, Demory M-E, Donners J, Vidale PL, Norton W, Shaffrey L, Stevens DP, Stevens I, Wood RA, Slingo J (2009) Impact of resolution on the tropical Pacific Circulation in a matrix of coupled models. J Climate 22: 2541–2556

Scaife et al (2008) The CLIVAR C20C project: selected twentieth century climate events. Clim Dyn 33:603–614. doi:10.1007/s00382-008-0451-1

Shaffrey LC et al (2009) U.K. HiGEM: The new U.K. High-resolution global environment model—model description and basic evaluation. J Climate 22:1861–1896. doi:10.1175/2008JCLI2508.1

Shukla J, Hagedorn R, Miller M, Palmer TN, Hoskins B, Kinter J, Marotzke J, Slingo J (2009) Strategies: revolution in climate prediction is both necessary and possible: a declaration at the world modelling summit for climate prediction. Bull Am Meteor Soc 90:175–178

Small RJ, Richards KJ, Xie SP, Dutrieux P, Miyama T (2009) Damping of tropical instability waves caused by the action of surface currents on stress. J Geophys Res 114:C04009. doi:10.1029/2008JC005147

Trenberth KE, Caron JM (2001) Estimates of meridional atmosphere and ocean heat transports. J Climate 14:3433–3443

von Storch J-S (2000) Signature of air–sea interactions in a coupled atmosphere-ocean GCM. J Climate 13:3361–3379

Wu R, Kirtman BP (2007) Regimes of local air-sea interactions and implications for performance of forced simulations. Clim Dyn 29:393–410

Wu R, Kirtman BP, Pegion K (2006) Local air-sea relationship in observations and model simulations. J Climate 19:4914–4932

Wu R, Kirtman BP, Pegion K (2007) Surface latent heat flux and its relationship with sea surface temperature in the national centers for environmental prediction climate forecast system simulations and retrospective forecasts. Geophys Res Lett 34:L17712. doi:10.1029/2007GL030751

Xie P, Arkin PA (1997) Global precipitation: a 17-year monthly analysis based on gauge observations, satellite estimates, and numerical model outputs. Bull Am Meteor Soc 78:2539–2558